NYE


UAG R-308

# GEOTHERMAL ENERGY RESOURCE INVESTIGATIONS AT MT. SPURR, ALASKA

**Donald L. Turner and Eugene M. Wescott**
**Editors and Co-Principal Investigators**

Submitted to:

**U.S. Department of Energy, Grant No. DE-FG07-841D2471**

**December 1986**


MT. SPURR, ALASKA, 1966 PHOTO BY AUSTIN POST

## EXECUTIVE SUMMARY

Spurr volcano is a composite Quaternary cone of largely andesitic composition located on the west side of Cook Inlet about 80 miles west of Anchorage and about 40 miles from the Beluga electrical transmission line (Figure 1-1). The south side of the cone is breached, with a small, Holocene, composite cone, Crater Peak, occupying this breach (Figure 1-2). The upper part of the volcano is a circular, 4.5 km-diameter flat region or basin, believed by some previous workers to possibly represent a caldera (Figure 1-2). Our geophysical surveys indicate that snow and ice depth exceeds 500 m in the deepest parts of the basin. The center of this summit depression is occupied by the small, Holocene, summit cone of Mt. Spurr.

Geologic mapping (Plate 1-1) shows that the present summit depression was produced by a Mt. St. Helens-type sector collapse, rather than by a caldera collapse. Geochronologic and previous tephrachronologic studies show that there has been an active magmatic system at Spurr volcano during the late Pleistocene-to-Holocene time interval that is of critical interest for geothermal energy resource assessment.

Surface geothermal manifestations include previously-unreported zones of fumarolic activity on the flanks of the Mt. Spurr summit cone, photographic evidence of snow melt at the summit crater, a previously-undescribed 40°C spring south of Crater Peak, and the fumaroles and hot crater lake of Crater Peak.

Major effort was devoted to geochemical and geophysical surveys of the accessible area south of Mt. Spurr, in addition to geologic mapping and geochronologic studies. Many coincident mercury and helium anomalies were found, suggesting the presence of geothermal systems at depth. Extremely

large electrical self-potential anomalies were also found, together with extensive zones of low resistivity discovered by our controlled-source audiomagnetotelluric survey. The juxtaposition of all of these different types of anomalies at certain areas on the south slope of Crater Peak (Plate 6-1) indicates the presence of a geothermal system which should be accessible by drilling to about 2000 ft. depth.

Follow-on studies should include passive seismic surveying to evaluate the possible presence of a steam system, together with additional electrical self-potential, helium and mercury surveys to better define the configuration and extent of probable reservoirs prior to exploratory drilling.

It is also evident that there is a strong volcanic hazard to be evaluated in considering any development on the south side of Mt. Spurr. This hazardous situation may require angle drilling of production wells from safer areas and placement of power generation facilities at a considerable distance from hazardous areas.

Two State of Alaska geothermal lease sales have been held in the Mt. Spurr area. The second sale was directly related to an earlier State release of the preliminary findings of our cooperative geothermal energy assessment investigations. A companion report on the detailed geology and geochemistry of Spurr volcano is currently in preparation by Dr. C. J. Nye.

TABLE OF CONTENTS

LIST OF ILLUSTRATIONS

Tables



Plates

Chapter 1

# The Mt. Spurr, Alaska Geothermal Energy Assessment Project: Introduction, Geologic Overview and Present Geothermal Manifestations

by

Donald L. Turner, Christopher J. Nye, James E. Beget and Eugene M. Wescott

## INTRODUCTION

Spurr volcano is a composite Quaternary cone of largely andesitic composition located about 80 miles west of Anchorage and about 40 miles from the Beluga electrical transmission line on the west side of Cook Inlet (Figure 1-1). Its upper regions are covered with ice and snow fields. The volcano is composed of andesitic flows and pyroclastics which overlie a basement of Tertiary-to-Cretaceous granite and quartz diorite (Reed and Lanphere, 1969). The south side of the cone is breached, with a small composite cone, Crater Peak, occupying this breach (Figure 1-2). The upper part of the volcano is a circular, 4.5 km-diameter flat region, resembling an ice-filled caldera. The center of this flat region is occupied by the present summit cone of Mt. Spurr, which appears to consist largely of a resurgent dome with some flows and tephras (Figure 1-2).

On July 9, 1953, Crater Peak erupted a large cloud of ash and steam to a height of 60-70,000 ft. Anchorage was covered with about 1/4 inch of ash, and ash fell as far away as Valdez.

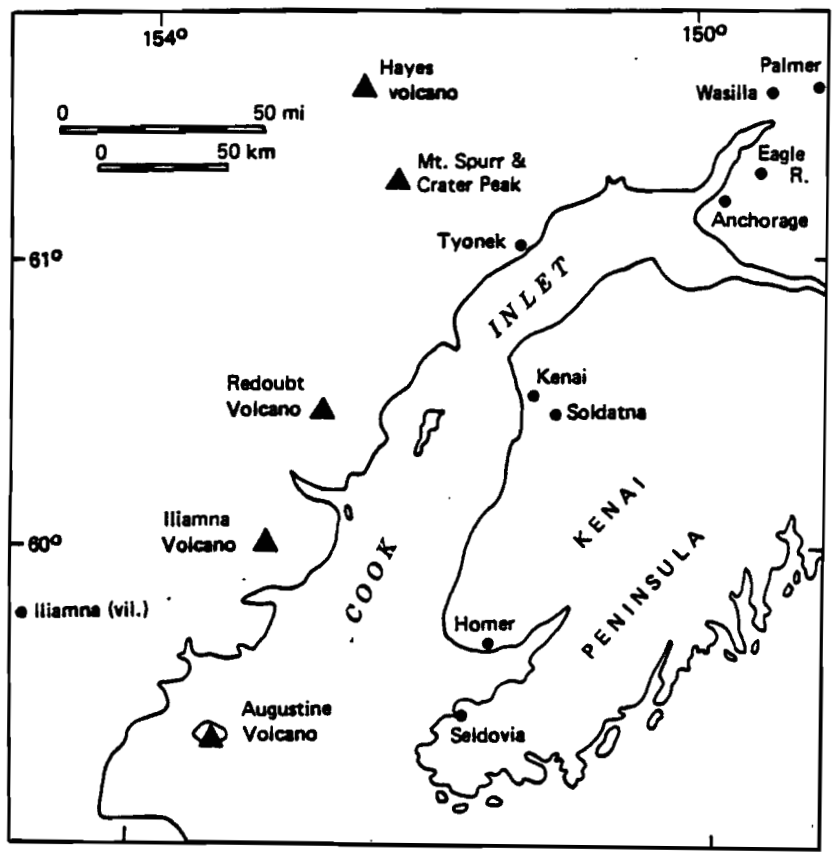


Figure 1-1. Locations of Quaternary volcanoes (triangles) in the Cook Inlet region of south-central Alaska (from Rhiele, 1985).


Figure 1-2. 1966 photo by Austin Post showing the present Mt. Spurr summit cone and the Crater Peak cone. Both cones are of Holocene age and were built after the summit of the original Spurr volcano was destroyed in a sector collapse event which sent a voluminous volcanic debris avalanche eastward down the Chakachatna River valley.

Capps (1935) suggested that Mt. Spurr might be a central cone built inside an older caldera, breached in places by glaciated valleys, although not all subsequent workers have agreed with this interpretation (Juhle and Coulter, 1955). A recent USGS radar echo sounding in the central ice field yielded an ice depth of 385 meters (R. March, personal comm., 1985). This result has caused further interest in the caldera hypothesis. Recent U-2 vertical stereo photography shows a circular summit depression that is also consistent with the caldera hypothesis.

An adequate geothermal energy assessment of this area requires that the caldera question be resolved. The presence of a caldera would indicate that the volcano had evolved a high level magma storage chamber. It is likely that large amounts of viscous and partially crystallized magma would be left in such a magma chamber following a caldera-forming eruption, resulting in a high-level heat source that could possibly produce one or more high temperature geothermal steam systems suitable for electrical power generation. Determining the age of this hypothetical eruption would be critical to determining whether or not the residual magma would have had sufficient time to cool and crystallize or, alternatively, whether it would still be hot enough to provide a viable geothermal energy resource. Initial USGS attempts to date valley bottom pyroclastics possibly associated with such an eruption have yielded "zero" K-Ar ages (J. Riehle, personal comm., 1985), suggesting that the hypothetical magma chamber could possibly be young enough to have retained significant amounts of heat up to the present time (see Geologic Overview for an alternative interpretation of these pyroclastic deposits).

## GEOLOGIC OVERVIEW

We have mapped six major volcano-stratigraphic units within the Mt. Spurr area (Plate 1-1). The first, and oldest, is a set of volcanic remnants which dip radially outward from near the present position of the Mt. Spurr summit. We have informally named these rocks the Older Flows and Tuffs Unit (OFT). This unit is composed of interbedded andesitic lava flows of diverse chemical and mineralogical composition, thick pyroclastic flows, dikes and sills. Based on the degree of glacial dissection, we originally suspected a mid-Pleistocene age, but our K-Ar dating has produced ages as young as 58,000 years for the stratigraphically highest flows in this unit (see Chapter 2).

The second unit consists of thin, interbedded basaltic andesite flows, named the Proto-Crater Peak flows. These flows are exposed in erosional remnants immediately east and west of Crater Peak. Flow bedding dips away from Crater Peak. We believe that these flows are from an ancestral Crater Peak, and that they were erupted during the early Holocene. Flow bedding in this unit is discordant to bedding in the OFT unit, and geologic mapping indicates that the Proto-Crater Peak flows were deposited in a pre-existing, major breach on the south side of the original Spurr volcano.

The third map unit comprises the basaltic andesite flows and thin tephras of Crater Peak itself, which is a small, thermally active, Holocene cone with a well-defined summit crater and crater lake (Figure 1-2). Both the Crater Peak and Proto-Crater Peak units contain many flows which are petrologically distinct from flows of the OFT unit because they contain abundant polycrystalline, monomineralic, clinopyroxene clots. Geologic mapping (Plate 1-1) shows that the Crater Peak cone was also built in the pre-existing south breach in the ancestral Spurr volcano. Rhiele (1985) has documented 35 tephra deposits produced by Crater Peak in the past 6,000 years.

The fourth unit comprises the summit peak of Mt. Spurr itself. This is a small, thermally active, conical peak in the center of the flat, circular snow field at the top of the mountain (Figure 1-2). Mt. Spurr is also a Holocene vent which has a breached, snow-filled crater. It is usually covered by snow, but we were able to collect a few acid andesite samples from areas which were snow free because the snow had been melted off by fumarolic activity. Available samples suggest that this unit is probably a resurgent dome, together with some flows and tephras.

The fifth unit is a 1000-foot thick pyroclastic unit referred to informally as the distal pyroclastics (Plate 1-1). This unit is composed of andesitic volcaniclastic flows with a few interbedded lava flows and avalanche deposits which fill the Chakachatna River valley south of Crater Peak. Because these flows fill what is otherwise a major, deeply glacially scoured valley, we believe that they are post-Pleistocene. However, these deposits are not characteristic of those produced during caldera collapse as we originally suspected. Rather than being a single, homogeneous deposit, this unit is composed of many discrete flows which differ from each other in mode of emplacement as well as in chemical and mineralogical composition. The dominant lithology is block-and-ash flows which are usually only a few meters, or a few tens of meters thick, although the valley south of Crater Peak exposes a flow several tens of meters thick. Some of the flows are subglacial hyaloclastites, which suggests that the whole unit was deposited over a significant time span, as the glaciers must have been at different stages of advance during different times of deposition.

The sixth unit is a voluminous, 3 km-wide volcanic debris avalanche deposit that extends approximately 11 km eastward from the south flank of Mt. Spurr down the Chakachatna River valley (Plate 1-1). This deposit

contains many coherent blocks up to several hundred meters across. These blocks consist of bedded lava flows and tephras believed to represent fragments of the original Spurr volcano transported downvalley. They are visible on the topographic maps as local knolls. In exposures along the Chakachatna River, the blocks are seen to be rotated and fractured. They lie in a matrix of less coherent, heterolithic volcanic debris, including much hydrothermally-altered material. One or more dacite ash flow tuffs similar in chemical composition to the Mt. Spurr summit cone are locally preserved on the surface of the debris avalanche deposit. The base of the deposit is not exposed anywhere along the river, which has cut down over 100 m into the deposit.

This unit covers about 30 $km^2$. Its minimum volume is 3 $km^3$, approximately equivalent to the estimated volume for the missing top of the original Spurr volcano. We interpret the volcanic debris avalanche deposit as having been formed by a Mt. St. Helens-type sector collapse of the original Spurr volcano in Holocene time. This concept is discussed more fully in the following section.

Caldera and Sector Collapse Hypotheses

The 4.5 km diameter, roughly circular ring of peaks and the relatively flat central snowfield surrounding the present summit of Mt. Spurr (Figure 1-2) suggest the possibility of caldera collapse. Due to the deep erosional dissection of the volcano, we were initially pessimistic about this hypothetical caldera being young enough for a shallow magma chamber to still be present today.

However, in light of the new K-Ar ages discussed in Chapter 2, we have revised our previous estimate of the age of the Mt. Spurr massif. The 58,000

year age from the stratigraphically highest dated sample of the OFT unit (85CNS35, Table 2-1) indicates that the ancestral vent which predates both the present Mt. Spurr summit cone and the Crater Peak cone (Figure 1-2) was active well into the late Pleistocene. This is recent enough that the basic morphology of the ancestral volcano should still be recognizable. However, the dated sample is from an isolated remnant of flows and tuffs whose bedding projects well above the present summit. There is therefore no presently recognizable source vent for these units. These observations lend considerable credence to the hypothesis that there has been recent collapse of the volcano. However, our recent work does not support the hypothesis that this collapse was a caldera-type event.

Geologic mapping and K-Ar dating (Plate 1-1) suggest that a St. Helens-type sector collapse of the original Spurr volcano has occurred, with collapse occurring to the south-southeast. Geologic mapping also shows that the collapsed southern margin of the ancestral volcano has been filled in later by the Proto Crater Peak lavas and the Crater Peak cone (Figure 1-2). We interpret the very large volcanic debris avalanche deposit between Straight Creek and the Chakachatna River (Plate 1-1) as the deposit formed by the proposed sector collapse. The volume of this deposit appears to approximate the estimated volume of material that would have been produced by sector collapse of the ancestral volcano.

The unglaciated ash flow tuff overlying the debris avalanche deposit may represent the juvenile magma which drove the eruption, and should be <10,000 years old. The unit proved undatable by the K-Ar method, as discussed in Chapter 2. Radiocarbon dating of a soil above the ash flow tuff only provides a much younger age limit of 495 ± 70 yr. (Geochron Labs, Lab No. GX-12072).

Since the proposed sector collapse mechanism could also account for the caldera-like form of the upper mountain (Figure 1-2), a separate episode of caldera collapse is not required to explain the present morphology. Caldera collapse, in the classic sense, would be expected to form voluminous ash flow tuffs. If caldera collapse post-dated sector collapse, unglaciated, voluminous, ash flow tuffs should have been well-preserved. There is no evidence for the existence of such units in the Mt. Spurr area. If caldera collapse had occurred earlier, there would have been no remaining high volcanic edifice to produce sector collapse. In summary, a single sector collapse event occurring in the last 10,000 years (post-Wisconsinan) followed by the building of the Crater Peak cone in the breached volcano rim and a resurgent dome with flows and tephras forming the present Mt. Spurr summit cone appear to be the simplest and most reasonable explanation for the observed geology and morphology of the Mt. Spurr area.

Although we have rejected the caldera collapse hypothesis, there is abundant evidence for a magmatic system in the Mt. Spurr area which has been active during late Pleistocene and Holocene time. This evidence will be discussed in the subsequent sections of this report. A more detailed discussion of the geology and geochemistry of the Mt. Spurr area will be given by Nye and others in a companion report which is currently in preparation.

## PRESENT GEOTHERMAL MANIFESTATIONS

There are several surface geothermal manifestations in the Mt. Spurr area. A previously-undescribed warm spring and a kilometer-long zone of warm seeps are located in the bottom of the N-S-trending valley immediately south of Crater Peak at the west side of the area explored with geophysical and

geochemical methods. A temperature of 40°C was measured at the spring in the eastern wall of the canyon about 3 m above the canyon floor. The estimated flow rate was 20 liters per minute. This water was analyzed by R. Motyka and the results will be discussed in a companion report in preparation by Nye and others. Most of the seeps are in the valley bottom and are extensively diluted with stream water. Total warm water flow for the entire valley bottom is probably on the order of 1000 liters/minute.

Crater Peak is quite active thermally. Air photo measurements indicate that its oval crater lake is about 220 m in longest dimension. The actual lake temperature was not measured, but it was just barely possible to leave a hand immersed in the water, suggesting a temperature of about 45°C. A very large fumarole is located near the north edge of the crater lake. This fumarole was estimated to be about 5 m in diameter. Its walls are vertical and covered with yellow sulphur. When observed on three separate occasions, it was emitting a large steam plume. The eastern side of the breached rim of the crater contains numerous small fumaroles and areas of steaming ground. Temperatures of seven small fumaroles in this area were measured at 96-98.5°C.

A one-day reconnaissance of the lower slopes of the Mt. Spurr summit cone revealed extensive areas of bare rock and fumarolic activity. Two geothermally-heated ribs of bare rock were exposed at the 10,000 ft. level. These were about 200 and 500 m long, respectively. Diffuse fumaroles are scattered along both. One 20 $m^2$ area of the larger rib had about 3-4 fumaroles/$m^2$. Actual fumarole temperatures were not measured, but they are believed to be at the pressure boiling point. The rock next to the fumaroles was too hot to touch.

Air photos taken of the Mt. Spurr summit cone crater in 1964 show clear evidence of subsidence caused by snow melt. A large semicircular depression

is present with a snow graben along one side. A dark pit in the center of the depression appears to be a lake formed by melting snow. The summit rim, which was snow-covered in the 1964 photos, showed areas of bare rock in 1985.

Three miles northeast of Mt. Spurr, at about the 9,500 ft. level, we observed a snow cave with icicles hanging from its mouth. Since snow does not usually melt at this altitude, the icicles may possibly suggest the presence of geothermal activity beneath the ice. Due to time constraints, we were unable to land the helicopter at the ice cave to conduct further investigations.

The observed geothermal manifestations indicate the presence of a north-south zone of hot ground extending from south of Crater Peak to north of Mt. Spurr.

## REFERENCES

Capps, S. R., 1935, The southern Alaska Range, U.S. Geological Survey Bull. 862, 101 p., 8 plates.

Juhle, R. W. and N. W. Coulter, 1955, Mt. Spurr (Alaska) eruption, July 9, 1953, Am. Geophys. Union Trans., 36(2):199-202.

Reed, B. L. and M. A. Lanphere, 1969, Age and chemistry of Mesozoic and Tertiary plutonic rocks in south-central Alaska, Geological Society of America Bulletin, v. 80, p. 23-43.

Riehle, J. R., 1985, A reconnaissance of the major Holocene tephra deposits in the Upper Cook Inlet region, Alaska Jour. of Volcanology and Geothermal Research, v. 26, p. 37-74.

Wescott, E. M., D. L. Turner, C. J. Nye, J. E. Beget and R. J. Motyka, 1985, Preliminary report on geothermal resource investigatons at Mt. Spurr, Alaska, Alaska Division of Geological and Geophysical Surveys Public Data File Report 85-65, 17 p., 5 plates.

Chapter 2

# Geochronology of Eruptive Events at Mt. Spurr, Alaska

by

Donald L. Turner and Christopher J. Nye

An accurate determination of the age of eruptive events is critical to the assessment of the geothermal energy resource potential of any volcanic system. At the beginning of this project, we had no way of knowing whether or not the Mt. Spurr andesitic flows would be old enough to be datable by the $^{40}K$-$^{40}Ar$ method. In fact, we suspected that most of the exposed sequence might be too young to date. Because of this anticipated problem, we decided to do a small pilot study to test for datability. Every effort was made to reduce laboratory air contamination during sample processing. The results of the pilot study were very encouraging and we proceeded to carry out an expanded dating program involving a total of 18 rock samples.

## Analytical Methods and Precision

All samples were dated as whole rocks. Potassium measurements were done in duplicate using $LiBO_2$ flux fusion and flame photometry with a lithium internal standard. Mineral standards were used to calibrate the photometer. Argon analyses were done by isotope dilution on a computerized, 6-inch-radius mass spectrometer. Analytical data for the $^{40}K$-$^{40}Ar$ age determinations are given in Table 2-1. Sample localities are shown on Plate 1-1.

Table 2-1. Analytical Data for $^{40}K$-$^{40}Ar$ Age Determinations of Whole-Rock Samples
Samples Are Arranged in Stratigraphic Order

| Stratigraphic Number | Field No. | Mean $K_2O$ (wt. %) | $^{40}Ar$ RAD (mol/g) X $10^{-11}$ | % $^{40}Ar$ RAD | Age (Ma) | ±1 Sigma (Ma) | |
|---|---|---|---|---|---|---|---|
| | | Ash Flow Tuff (Ages believed to be too old due to excess $^{40}Ar$) | | | | | |
| AF-09 | 85CNS09 | 1.72 | .0183 | 0.64 | *≥.074± | .024 | |
| AF-08 | 85CNS08 | 1.65 | .0330 | 1.75 | *≥.139± | .014 | |
| AF-06 | 85CNS06F | 1.64 | .0150 | 0.75 | *≥.065± | .016 | |
| | | Crater Peak Flows (Ages indeterminate) | | | | | |
| CP-06 | 85CNS10 | .737 | .0051 | 1.19 | .049± | .045 | |
| CP-01 | 85CNS15 | 1.23 | .0044 | 0.62 | .025± | .024 | |
| | | Proto Crater Peak Flows (Age indeterminate) | | | | | |
| PCP-B07 | 85CNS27F | 1.25 | .0050 | 1.07 | .028± | .029 | |
| | | Older Flows and Tuffs | | | | | |
| OFT-A08 | 85CNS35 | 1.33 | .0128 | 2.71 | .063± | .018 | |
| OFT-A08 | 85CNS35 | 1.33 | .0105 | 2.54 | .054± | .011 | |
| | | | | | $\bar{X}_2$= .058± | .018 | |
| OFT-A06 | 85CNS37 | 1.58 | .0194 | 6.57 | .085± | .009 | |
| OFT-A05 | 85CNS21 | 1.67 | .0266 | 10.3 | .110± | .006 | |
| OFT-A04 | 85CNS22 | 0.701 | .0135 | 2.09 | *≥.134± | .021 | |
| OFT-A02 | 85CNS24 | 1.61 | .0259 | 8.26 | .112± | .008 | |
| OFT-B10 | 85CNS40 | 1.44 | .0246 | 8.18 | .119± | .016 | |
| OFT-B10 | 85CNS40 | 1.44 | .0238 | 7.36 | .115± | .012 | |
| | | | | | $\bar{X}_2$= .117± | .016 | |
| OFT-B08 | 85CNS42 | 1.34 | .0269 | 3.07 | .139± | .009 | |
| OFT-B05 | 85CNS55B | 1.79 | .0167 | 1.73 | .065± | .015 | (Sill?) |
| OFT-B01 | 85CNS59 | 1.67 | .0645 | 3.53 | .255± | .052 | |
| OFT-26 | 85CNS26 | 1.36 | .3886 | 3.93 | †≥2.08± | .20 | |

Constants: $\lambda_\varepsilon+\lambda_\varepsilon' = 0.581\times10^{-10}$ yr$^{-1}$, $\lambda_\beta = 4.962\times10^{-10}$ yr$^{-1}$, $^{40}K/K$ total $= 1.167\times10^{-4}$ mol/mol

Notes: Ages preceeded by ≥ are minimum ages based on thin section observation of groundmass glass (*) and/or minor alteration (†). RAD = radiogenic, Sigma = standard deviation

With two exceptions, the argon analyses represent single sample fusion-gas extraction experiments. As a general procedure, the gas samples were split into 2-4 aliquots and these were run sequentially on the mass spectrometer. The first split was used to "flush" the spectrometer in order to reduce the well-known memory effect in static gas analysis. This effect is particularly important when analyzing young samples with small amounts of radiogenic $^{40}Ar$, such as the Mt. Spurr rocks. Results from these "flushing splits" were not averaged in with the subsequent splits unless they were statistically equivalent. The results from the remaining splits were averaged to calculate the values of radiogenic $^{40}Ar$, % radiogenic $^{40}Ar$ and age given in Table 2-1.

As a test of reproducibility, two rock samples were split and had duplicate sample fusion-gas extraction experiments performed several months after the initial analyses. The results (.063±.018, .054±.011 and .119±.016, .115±.012, Table 2-1) agree well, indicating that our results are reproducible.

Analysis of Validity of Ages Obtained from the Older Flows and Tuffs Unit

The replicate analyses discussed above indicate that our results are reproducible for rocks within the Older Flows and Tuffs Unit (OFT) that are old enough to date by the K-Ar method. Reproducibility (precision) is important, but says nothing about the accuracy (degree of approximation to the actual times of solidification and cooling) of the ages obtained for the dated lava flows. Moreover, the K-Ar dating of rocks as young as the apparent ages of many of our Mt. Spurr samples is generally considered to be extremely difficult. An independent test of geological accuracy is therefore required before these ages can be accepted as valid.

We argue that the ages from the OFT are valid based on the excellent agreement of ages obtained with the observed stratigraphic sequence of the dated samples. This argument is illustrated by Table 2-1, which lists the samples in stratigraphic order, with the youngest at the top. Nine of the ten ages from the OFT unit are in excellent agreement with the observed stratigraphy. The remaining sample (OFT-B05) is significantly younger than five dated flows which overlie it. We suggest that this sample may be a sill that was mistaken for a lava flow in the field.

Analysis of Ages Obtained From Younger Units

Two samples from the Crater Peak flows and one sample from the Proto Crater Peak flows were dated. For all three analyses, the standard deviations are as large as the apparent ages, indicating that the ages are indeterminate (Table 2-1).

Three samples were dated from the same outcrop of the ash flow tuff unit (Plate 1-1). This outcrop is a crystal vitric tuff representing a single eruptive event. The tuff overlies the volcanic debris flow unit (Plate 1-1) believed to represent material derived from the sector collapse of the ancestral Mt. Spurr volcano (see Chapter 1). The debris flow unit has an extremely hummocky surface, indicating that it has never been glaciated. Geomorphic evidence indicates that major glaciation occurred in this same area until the end of the Pleistocene. The unglaciated debris flow and its overlying ash flow tuff are therefore believed to be no older than 10,000 years. The measured apparent ages varied between 65,000 and 139,000 ± 16-24,000 years. The combination of the geologic improbability of these ages, together with the highly variable (nonreproducible) radiogenic $^{40}Ar$ contents (Table 2-1) of the three samples from the same outcrop are strong evidence for

incomplete degassing of pre-existing magmatic argon during the eruption process. This "excess argon" would be expected to be heterogeneously distributed in the quickly-cooled groundmass glass and would therefore produce highly variable ages for the same material, all of which would be significantly older than the eruptive event. We conclude that the 65,000-139,000 yr apparent ages are erroneously old due to excess argon and have no geologic significance.

We attempted to date two samples (85CNS01,39) from the Distal Pyroclastics Unit (Plate 1-1). Both attempts were unsuccessful, with the extracted gas consisting entirely of atmospheric argon. These analyses are not listed in Table 2-1.

Geochronology of Eruptive Events

Our K-Ar results, together with geologic mapping by Nye and Beget (Plate 1-1) and data from Riehle (1985) indicate the following chronology of eruptive events:

| Ages (years) | Event |
|---|---|
| 1953 | Crater Peak ash eruption (Historically documented) |
| < 6,000 | Crater Peak ash eruptions (35 tephras in 6,000 yrs, Riehle, 1985) |
| <10,000 | Extrusion of present Mt. Spurr summit cone (resurgent dome, flows and tephras) |
| <10,000 | Distal Pyroclastics |
| <10,000 | Crater Peak lava flows |
| <10,000 | Proto Crater Peak lava flows |
| <10,000 | Sector Collapse:<br>Silicic ash flow tuff overlying debris flow (may represent the juvenile magma that drove the sector collapse event)<br>Volcanic debris avalanche (interpreted as a deposit of material from the sector collapse event) |
| 58,000 ± 18,000 to 112,000 ± 8,000 | Upper older flows and tuffs unit (OFT) |
| 117,000 ± 16,000 to 255,000 ± 52,000 | Lower OFT |
| 2,080,000 ± 200,000 | Oldest exposed OFT (could possibly be unrelated to the ancestral Mt. Spurr volcano) |

We now have good evidence that the Mt. Spurr volcanic system was active at least as often as 2,080,000; 255,000; 139,000; 117,000-85,000, and 58,000 years before present, in addition to the numerous younger magmatic events listed in the above table (Holocene Proto Crater Peak flows, Crater Peak flows, ash flow tuff, distal pyroclastics, Mt. Spurr summit cone and the 35 Crater Peak tephras shown in Figure 2-1. This documentation of extensive magmatic activity during late Pleistocene and Holocene time indicates the presence of a magmatic system at Mt. Spurr during the late Pleistocene-to-Holocene time interval that is of critical interest for geothermal energy resource assessment.

## REFERENCES

Riehle, J. R., 1985, A reconnaissance of the major Holocene tephra deposits in the Upper Cook Inlet region, Alaska, Jour. of Volcanology and Geothermal Research, v. 26, p. 37-74.

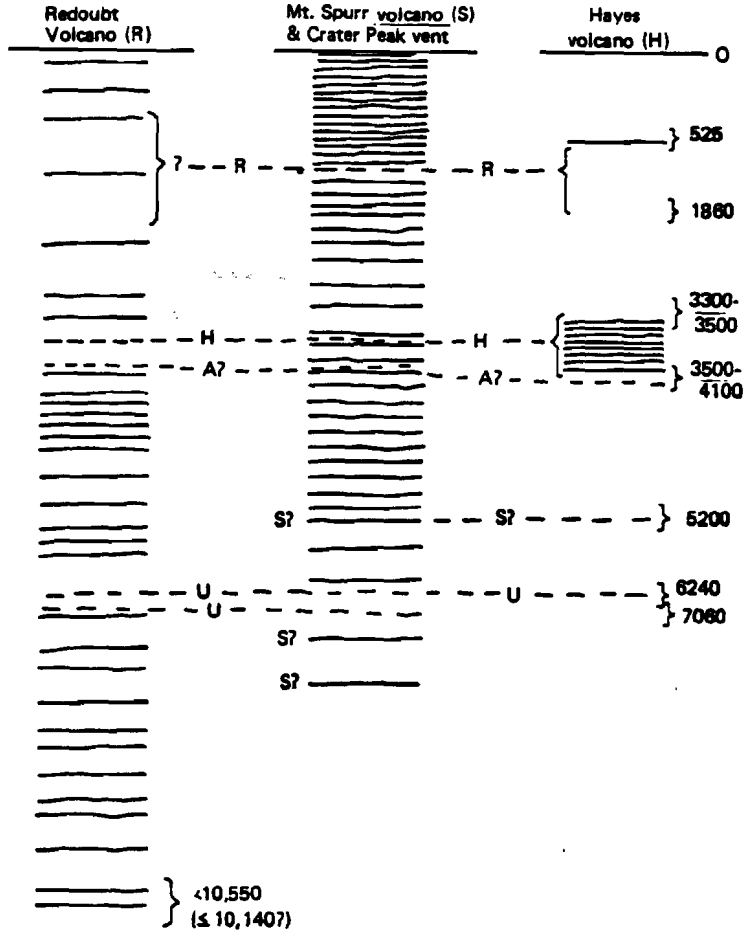


Figure 2-1. Chronologic diagram summarizing those Holocene eruptions of the upper Cook Inlet volcanoes which produced major, east-directed tephra deposits. Each solid line under a particular heading represents an eruption of that volcano; absolute ages are based on available radiocarbon data. Sources of the regional deposits, which are indicated by horizontal dashed lines, are as follows: Augustine Volcano (A), Redoubt Volcano (R), Spurr volcano (S), Hayes volcano (H), and uncertain (U). A vertical bracket denotes uncertainty of absolute age, uncertainty of correlation of a regional tephra deposit with a particular reference sample, or both. From Riehle (1985).

Chapter 3

# Ice Thickness Measurements in the Basin Surrounding the Summit of Mt. Spurr, Alaska

by

Eugene M. Wescott, William Witte, Patricia Moore and Keith Echelmeyer

## INTRODUCTION

One of the research aims of the 1985 field program on Mt. Spurr was to investigate the ice thickness in the roughly circular area surrounding the Mt. Spurr summit cone (Figure 1-2). The area is rimmed by isolated rock peaks and walls separated by several glaciers. The hypothesis we tested was that the original Spurr volcano collapsed, forming a caldera, and that later the present Mt. Spurr summit cone was built up in roughly the center of the resulting depression. At the present time the area is covered with snow and ice, obscuring the evidence for or against the caldera hypothesis.

We employed two techniques to determine the ice depth and thus the configuration of the rock surface beneath. The first was radio echo sounding and the second was a one-frequency, magnetotelluric measurement using the VLF signal from the U.S. Navy transmitter in Hawaii.

Radio Echo Sounding of Glacier Thickness

A mono-pulse ice radar was used to measure the ice thickness. The radio pulse has a center frequency of 5.5 MHz with a pulse repetition rate of several hundred hertz, and each pulse is limited to 1-2 cycles. The pulse is transmitted into the ice through a resistively-damped dipole antenna 20 m long which is laid out on the ice surface. At the same time a pulse is transmitted into the ice, an air wave propagates along the surface to the receiving antenna approximately 60 m away. The air wave triggers an oscilloscope. Meanwhile the pulse within the ice may encounter one or more reflecting surfaces (an interbed or the glacier bed) where a fraction of the radio wave is reflected back towards the surface. Multiple reflections can occur from different parts of the bed or different internal layers, sometimes leading to a complex wave train. The oscilloscope screen is photographed for a permanent record of the arrivals.

The distance to a reflector can be determined once the time interval between the arrival of the air wave and the reflected wave is known. In temperate ice the velocity of the radio waves is 168 m/μ sec. Due to the geometry of the transmitter and receiver dipoles, the reflector is constrained to lie somewhere on an ellipsoid. Given a sufficiently close-spaced number of data points across the surface of an ice mass, the envelope of these reflection ellipsoids defines a bottom (or interbed) profile, but if the data are sparse, it is sometimes difficult to judge which arrivals are from the reflector.

Other problems inherent in the method are the relatively low power emitted which limits the measurable ice depth to 700-800 m. Water inclusions can severely attenuate the signal as well, reducing the effective depth of operation. When the returns are clearly defined, the measurement precision is about ±5 m.

## The Mt. Spurr Icefield Survey

Weather limited the amount of data which could be obtained in our survey. The helicopter could not safely transport people to and from the ice-field except when the weather was very good, and it was unsafe to shut off the engine on top of the mountain. These considerations limited the radar and VLF measurements to less than two days. First attempts at radio echo soundings were on the south-southwest side of Mt. Spurr between Spurr and Crater Peak. No usable echoes were obtained. On a second day, the 18 sites shown on Figure 3-1 were occupied, with 15 producing usable echoes. Several sites produced multiple echoes, and most of the indicated depths were less than 100 m. The mean conformation of the deeper travel times is shown on the contours. It shows a generally bowl-shaped basin opening to the northeast. None of the depths we measured are nearly as deep as a single USGS measurement of 385 m (1262 ft) taken in 1984 (R. March, personal communication, 1985), or as deep as indicated by the VLF-EM-16-R data discussed below. Thus we think that the reflections are likely to be from a major ash layer deposited in the 1953 eruption of Crater Peak (see Chapter 2) rather than from the glacier bed, except near the edges of the ice field.

## VLF Ice Depth Measurements

The Geonics Ltd. EM-16-R VLF resistivity meter can be used to estimate the resistivity of the earth or glacial ice and snow by measuring the electric (E) and magnetic field strength (H) of one of the high-power VLF transmitters located at various sites around the world. The $E_x$ field component is measured from a pair of electrodes placed in the ground or snow 10 m apart directed in line with the transmitter while $H_y$ is measured with a horizontal coil at right

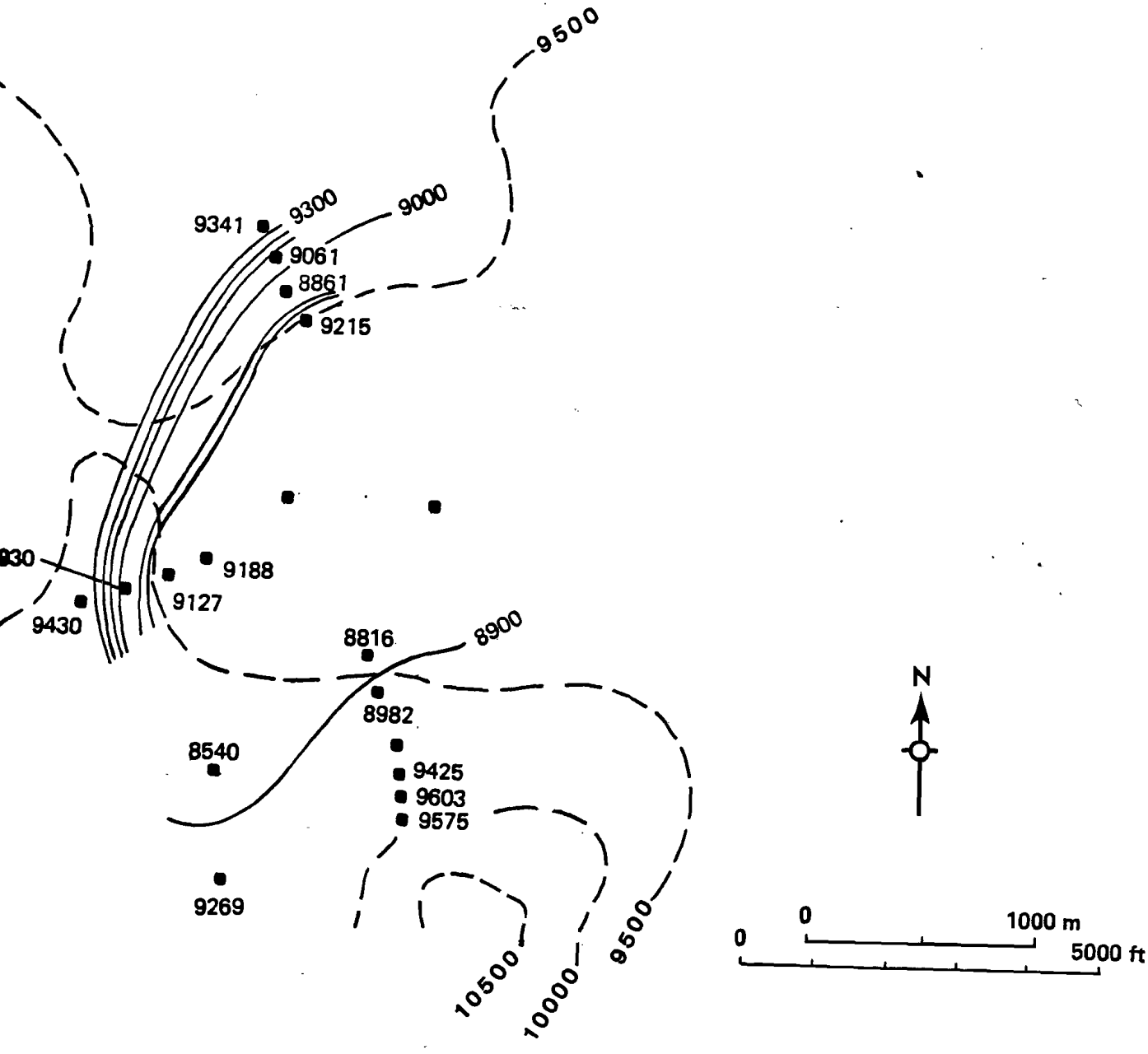


Figure 3-1. Map of northwest section of the upper Mt. Spurr basin showing sites where radio echo soundings were attempted and contours of the elevations of the deepest reflections. Numbers at stations are elevations of deepest reflections. We interpret this map as representing the configuration of the 1953 Crater Peak tephra layer incorporated within the ice, rather than a bedrock surface.

angles to $E_x$. By rotating two dials to obtain an audio null, apparent resistivity in ohm-meters (Ω-m) and the phase angle between the perpendicular electric ($E_x$) and magnetic ($H_y$) components can be read directly. The apparent resistivity is the Cagniard or magnetotelluric resistivity at the frequency of 20 kHz: $\rho_a = 10^{-5}|E_x/H_y|^2$ in Ω-m, where E is in mV/km and H is in gammas. There is a small correction necessary for frequencies different than 20 kHz.

From the upper glacier fields of Mt. Spurr there was an unobstructed line of sight towards the U.S. Navy VLF transmitter NPM at Lualualei, Hawaii, broadcasting at 23.4 kHz. The signal was strong enough to obtain good nulls in both resistivity and phase. The electrodes were placed in the firm snow. Readings were made at the same sites as the impulse radar soundings and at a few other sites in addition.

Grissemann and Reitmayr (1978) have developed an algorithm for inverting field data for a two-layer earth model. There are three variables: the resistivities of the top and infinite underlying layer and the thickness of the top layer. The two measured quantitites are the apparent resistivity and the phase angle. This resolves into two equations with three unknowns. If any one of the three unknowns is known or assumed, then the other two can be determined.

The resistivity of snow and glacial ice has been measured at various sites around the world using galvanic resistivity techniques. Röthlisberger and Vögtle (1967) reported values on wet Swiss glaciers ranging from 5 to $30 \times 10^6$ Ω-m. The measured values on dry Antarctic glaciers are lower and fall in a very narrow range of 0.4 to $2.0 \times 10^5$ Ω-m when the temperature is between -2 and -29°C (Reynolds and Paren, 1984; Reynolds, 1982). The snow and ice of Mt. Spurr may not fit into either class of glacier because of fumarolic gasses containing $H_2S$ and the possibility of episodic ash falls being incorporated

into the ice. The combination of water in clouds enveloping Mt. Spurr and sulphur in the fumarolic gasses should result in a sulphuric acid component being added to the snow and, eventually, to the ice, thus lowering its resistivity.

We did make a few Schlumberger array resistivity measurements on the Mt. Spurr ice field. We had to operate under adverse conditions near sunset with a cold wind blowing. We managed to obtain readings at six 1/2 AB spacings ranging from 1 to 100 m. We used a 90-volt battery pack connected to aluminum stakes in the snow as current source, and measured the potential difference across a pair of $Cu\text{-}Cu_2SO_4$ porous pot electrodes with a high impedance digital voltmeter. Both the current and the potential decayed with time. We attempted to read simultaneous values of each to calculate the resistivity. The calculated apparent resistivity values are too irregular to make a good fit to standard curves or to use with an automatic curve fitting program. The near-surface resistivity is about $2.2 \times 10^6$ Ω-m, but the deeper resistivity decreases steeply and was about 50,000 Ω-m at our longest 1/2 AB spacing of 100 m. It is a reasonable assumption that the ice resistivity decreases further with depth, and that the average value over a thickness of a few hundred meters may be much lower than 50,000 Ω-m.

To begin calculations, we assumed various resistivity values from $10^6$ to $10^4$ Ω-m for the snow and ice layer, then calculated the corresponding depths to bedrock and the resistivity of the rock. In every case, as we decreased the input resistivity of the snow and ice, the depth to bedrock increased and the rock resistivity decreased. The rock resistivity started very high (~ 10,000 Ω-m) at ρ ice of $10^6$ and approached limiting values near 0 Ω-m as the snow and ice resistivity was in the range 9900 to 33,000 Ω-m.

The controlled-source audio-magnetotelluric measurements we made on the south side of Crater Peak (Chapter 4) showed that a resistivity near 100 Ω-m is a typical value for the near-surface rock resistivity of the volcano. Because all exposed rocks are geothermally heated on the Mt. Spurr summit cone (Chapter 1), there is reason to believe that the rock underlying the snow and ice contains unfrozen water which may be high in disolved ions. A value of 100 Ω-m for the rock underlying the ice is not unreasonable in this situation. We have therefore assumed this value and recalculated the resisitivity and thickness of the snow and ice. The mean value of the recalculated ice resistivity was 17,900 ± 5260 Ω-m, using 17 datum points.

Results

The results of the EM-16-R soundings are shown in Figure 3-2 as a contour map of the bedrock under the ice. The data suggest a cirque-like basin north of Mt. Spurr open to the east. There is a nearly flat area on the snow surface between Mt. Spurr and a narrow, north-south-trending, snow-covered ridge. The thickness of snow and ice in the center of this area measured with the EM-16-R is 335 m (1100 ft), but structural mechanics require that the narrow, north-south ridge must be supported by rock less than 60 m below the surface (W. Harrison, personal communication). Figure 3-3 shows a cross section including the VLF-measured surface and the projected rock ridge. This is suggestive that the ridge could be a remnant wall produced by caldera or sector collapse of the top of the original volcano.

Figure 3-4 is a profile north-northwest from the peak of Mt. Spurr showing the present snow and rock surfaces, the VLF-calculated bedrock surface and the radar reflection surfaces. Close to the edges of the basin where rock outcrops, the VLF and radar depths are similar. But in the basin, the VLF

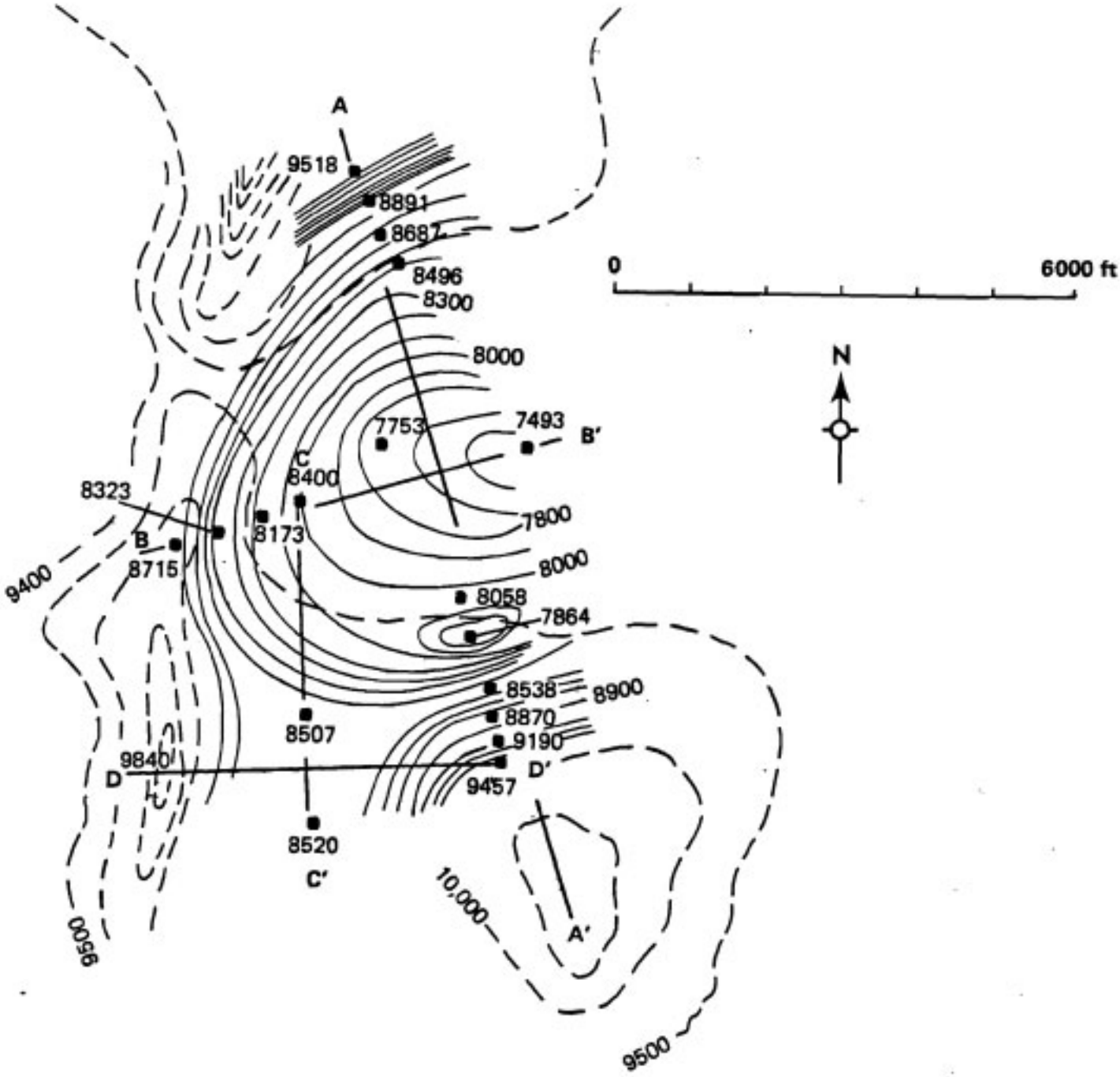


Figure 3-2. Map of northwest section of the upper Mt. Spurr basin showing elevation contours of bedrock under the ice derived from VLF resistivity measurements and calculations using 100 Ω-m as the average resistivity of the bedrock. Dashed contours represent surface snow and ice or exposed rock topography. Cross section lines are also shown.

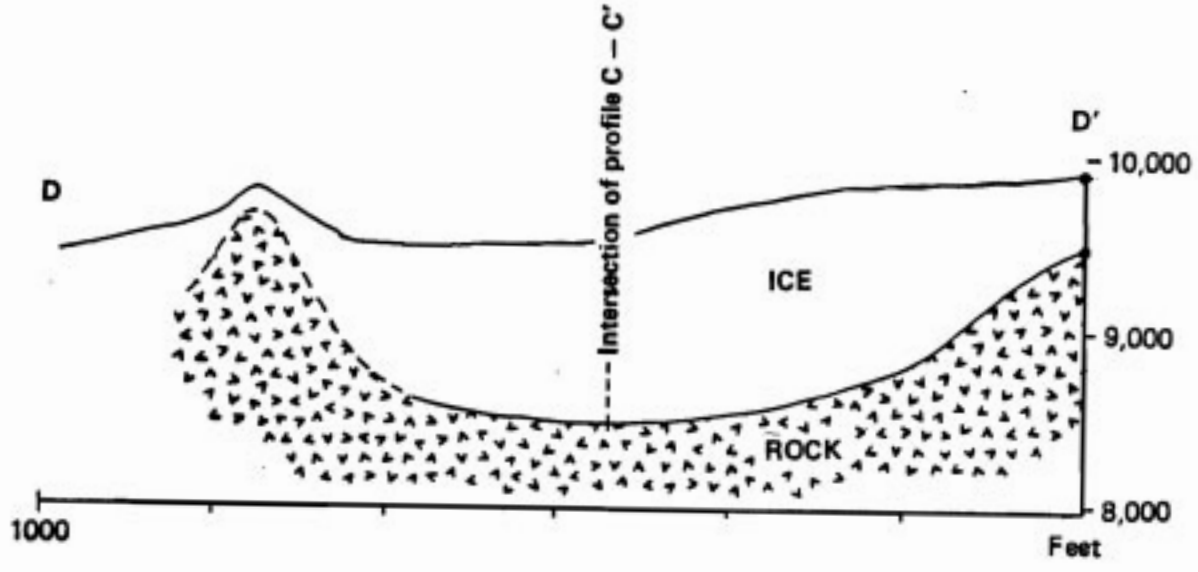


Figure 3-3. Cross section DD' based on VLF resistivity data showing the maximum depth to the narrow rock ridge underlying the ice.

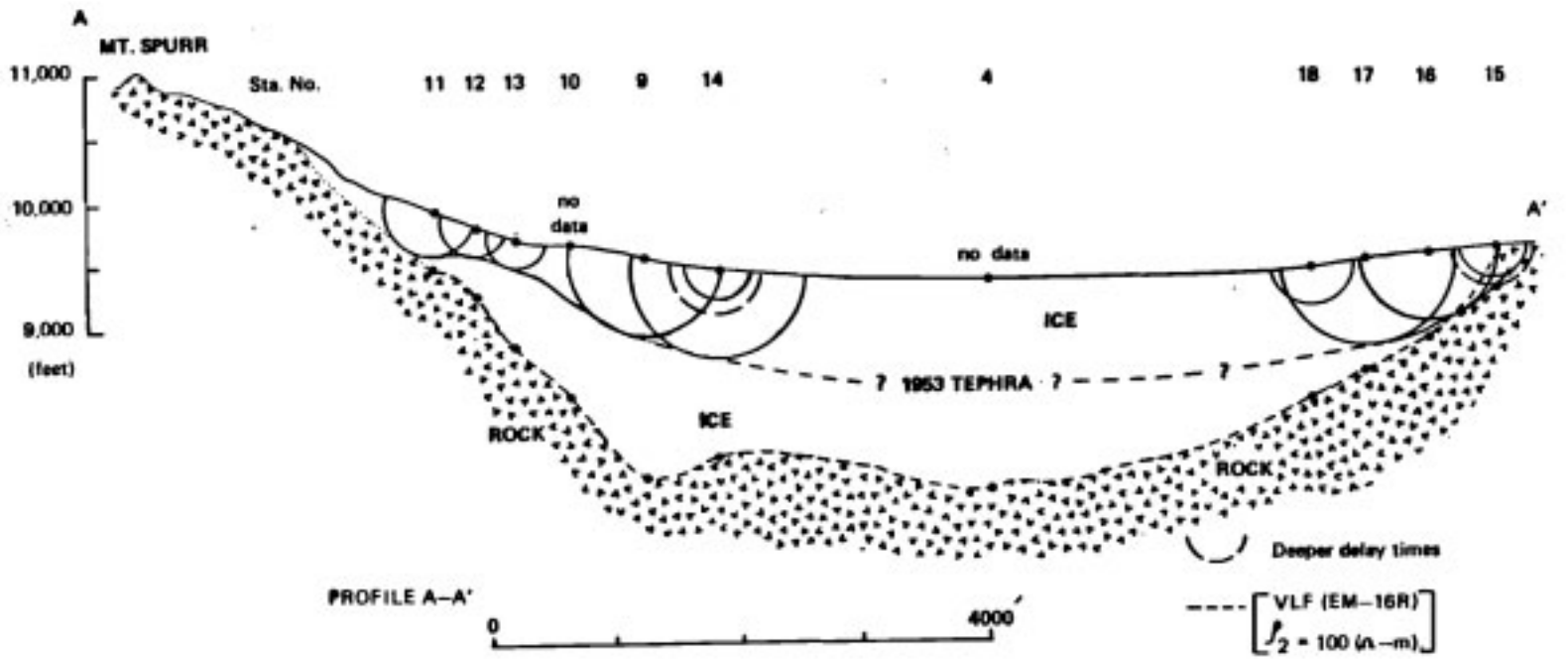


Figure 3-4. Profile AA' of the VLF resistivity-calculated bedrock surface and the radar reflection surfaces. Radar reflections are interpreted as representing the 1953 Crater peak tephra layer.

depths are much greater than the radar values. Some radar measurements produced multiple reflections. We hypothesize that the radar reflections in the basin are from ash layers -- principally the 1953 Crater Peak tephra (Chapter 2), and not bedrock reflections. Figure 3-5 shows profiles B-B' and C-C' across the basin, also showing, with one exception at site 2, no radar reflections from the bottom.

## Summary and Conclusions

The radar reflections we obtained were generally much shallower than the single radar measurement of 385 m in the same area obtained by the USGS (R. March, personal communication, 1985). We conclude that our mid-basin radar measurements were from the 1953 Crater Peak ash layer incorporated within the ice. The EM-16-R VLF depth estimates depend on the assumption of 100 Ω-m for the uniform resistivity of the underlying rock. From experience we know that the volcano is very heterogeneous, and undoubtedly has areas of higher and lower resistivity. But even if our estimate is off by an order of magnitude either way, the VLF depths would only be off by 10% and would still be much greater than the radar depths. The USGS radar depth of 385 m is close to our VLF depths. We conclude that the estimated depth of snow and ice in the center of the basin exceeds 500 m. Our maximum VLF depth is 575 m. These ice depth measurements, coupled with the inferred, near-surface narrow rock ridge (shown in Figure 3-3), are consistent with Spurr volcano having a major summit depression produced by a summit collapse episode which preceeded the formation of the present Mt. Spurr summit cone. Both caldera collapse and Mt. St. Helens-type sector collapse are possible mechanisms for producing the observed summit depression. Geologic arguments favoring the sector collapse mechanism are discussed in Chapter 1.

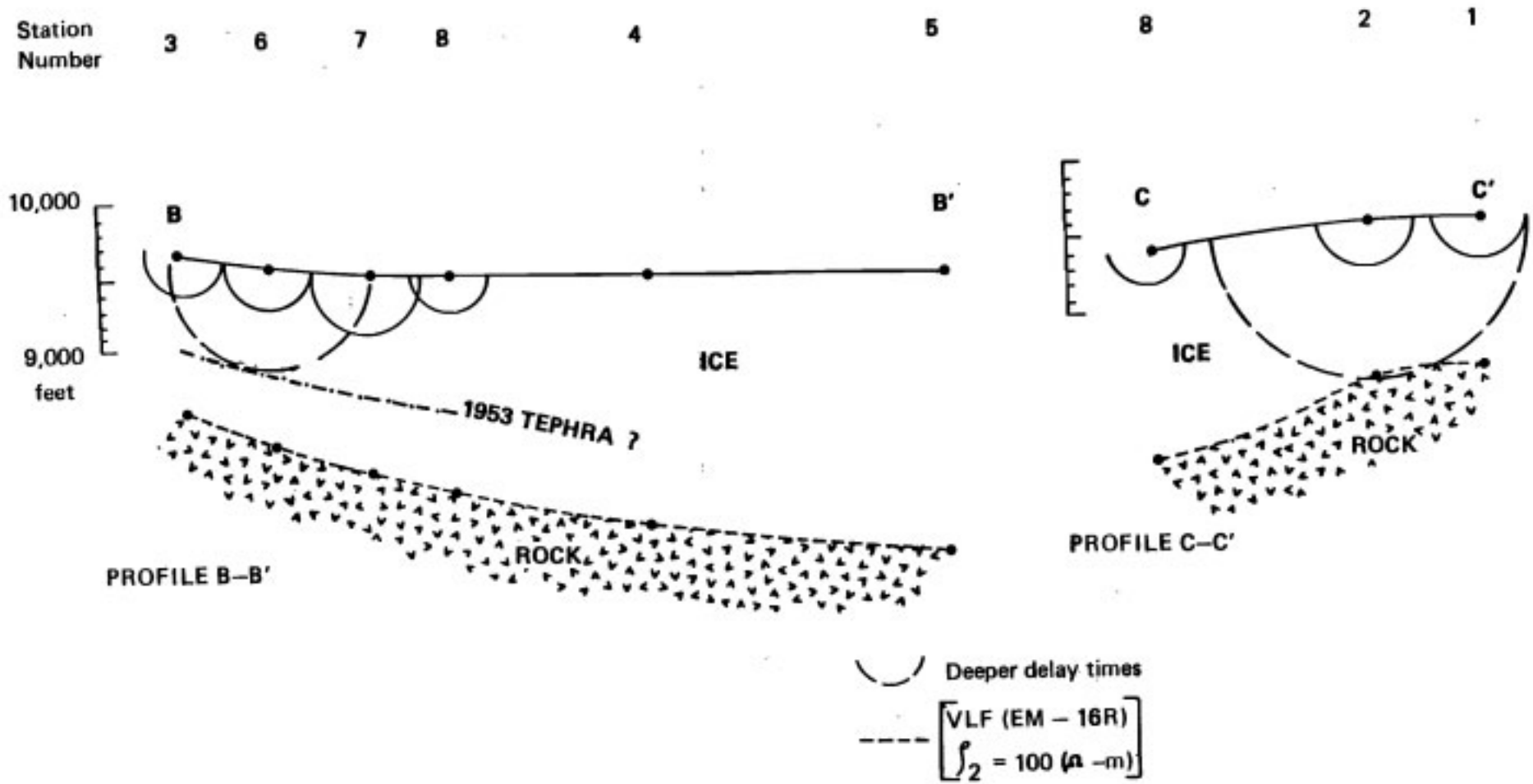


Figure 3-5. Profiles B-B' and C-C' of the VLF resistivity-calculated bedrock surface and the radar reflection surfaces. Radar reflections are interpreted as representing the 1953 Crater Peak tephra layer.

## REFERENCES

Grissemann, C. and G. Reitmayr, 1978, VLF magnetotellurics in ore exploration and structural geology (abstract), Society of Exploration Geophysics Meeting, San Francisco.

Reynolds, T. M., 1982, Electrical resistivity of George VI Ice Shelf, Antarctica Penninsula, Annals of Glaciology, 3, 279-283.

Reynolds, J. M. and J. G. Paren, 1984, Electrical resistivity of ice from the Antarctic Penninsula, Antarctica, Journal of Glaciology, 30(106), 289-295.

Röthlisberger, H. and K. Vögtle, 1967, Recent D.C. resistivity soundings on Swiss glaciers, Journal of Glaciology, 6(47), 607-621.

Chapter 4

# Electrical Geophysical Surveys for Potential Geothermal Reservoirs on the South Side of Mt. Spurr, Alaska

by

Eugene M. Wescott, William Witte, Patricia Moore and Donald L. Turner

## SELF-POTENTIAL SURVEY

### Introduction

The first reconnaissance electrical method used on the southeast flank of Crater Peak was the self-potential, or spontaneous potential, method of geophysical prospecting which involves measuring the electrical potential (voltage difference) at points on the ground with respect to a reference point. To minimize spurious electrochemical voltages between the contacting electrodes and the ground, non-polarizing electrodes must be used. These consist of a metal and one of its soluble salts in a concentrated solution such that metal atoms may move reversibly into solution from, or plate onto, the metal electrode in response to an electric field. A copper electrode in a saturated copper sulfate solution contained in a porous cup is the most common electrode. A very high input impedance voltmeter is used to measure the voltage between electrode pairs.

The preferred measurement technique is to use a fixed electrode as a reference point, and a long wire to a second electrode which is moved to

stations in a grid in the area to be surveyed. If a large area is to be surveyed, or the terrain or vegetation make the use of a long wire impractical, a pair of electrodes with a shorter separation may be leap-frogged around the area to measure the gradient. By summing the gradient a potential map or profile can be produced.

Self-potential anomalies may be the result of several natural and man-made processes. Conductive deposits of pyrite, pyrhotite, other sulfide minerals, magnetite, covelite and graphite are known to generate self-potential anomalies which are almost always negative in polarity over the top of the body. The conducting body is theorized to serve as a path for electrons from the reducing environment below the water table to the oxidizing zone above. These anomalies are usually confined to a few hundred meters in width and about 100 mV (millivolts) in amplitude. Buried well pipes and pipelines also produce self-potential anomalies by pipe corrosion.

Self-potential anomalies that appear to be related to geothermal activity have been reported from a considerable number of geothermal areas (Corwin and Hoover, 1979). Anomalies range from 50 to 2000 mV in amplitude over distances of 100 m-10 km. Their wave forms and polarities vary widely. Steep gradients are often observed over the trace of faults which are thought to act as conduits for thermal fluids. Republic Geothermal (1983) reported 3 self-potential anomalies near Makushin Volcano, Alaska of -600 mV, -500 mV and a dipolar anomaly of ± 100 mV amplitude. Subsequent drilling on the -500 mV anomaly confirmed its geothermal origin.

The flow of water through permeable rocks produces charge separation, and a significant self-potential phenomenon called the electrokinetic effect. This effect has been cited as the explanation for large anomalies over hot zones. Zablocki (1976) reported on the results of self-potential field tests

in Kilauea, Hawaii, and concluded that they were the single most useful geophysical method for identifying and delineating thermal anomalies. He found positive potential differences as high as 1600 mV across distances of a kilometer or less over known fumarolic areas and recent eruptive fissures.

Morrison et al. (1978) found that the voltage - pressure relationship in the electrokinetic effect decreases with increasing salinity and increases with temperature. For a saline solution similar to the brine at the important geothermal field at Cerro Prieto, Mexico, a pressure difference of 100 atmospheres at 24°C across reservoir core samples would generate a maximum potential of 40 mV with the lower pressure side positive with respect to the high pressure side. As temperature increased, the potential increased to an expected 200 mV at 300°C.

Temperature differences also produce self-potential anomalies through thermoelectric coupling (Morrison et al., 1978). A typical coupling coefficient for sandstones is 0.060 mV/°C with the hot side positive with respect to the cold side. For a typical Cerro Prieto core and brine and a 300°C temperature difference, 18 mV would be produced by the temperature effect alone.

Potential differences can also be produced by differences in ionic concentrations in the formation fluids amounting to about 25 mV per power of 10 concentration difference (Sill, personal communication, 1982). This can be significant if there are major lateral concentration changes in the ground water.

Self-Potential Survey

The area on the south flank of Mt. Spurr, specifically on the south side of Crater Peak, is essentially free of brush, and we were able to use the long wire technique from a fixed reference electrode to carry out the survey. Some survey work was done on the plateau to the east where the camp was located, and we planned to tie to the main survey. However, it proved to be too difficult to traverse either the glacier or the canyon separating the two areas. As the camp area survey was too limited to be significant, we present only the Crater Peak data.

We set up a 100 m dipole in camp to continuously record telluric currents. If the activity was too high at daybreak, other activities than S-P were scheduled for the day. We used fine copper magnet wire (32 or 34 gauge) as the long wires. Positions of stations were determined from map and air photos and by use of pocket altimeters and pacing. Traverses either started near the top of the area and ran downhill or contoured. Most traverses tied to previous traverses within 100 mV.

There was a very strong topographic effect (TE) in the self-potential data. Using a least squares fit, we found the TE to be -151 mV/100 m elevation change. TE has been well known to geophysicists for more than 70 years (Ernstson and Scherer, 1986). The explanation favored at this time is that this effect is due to streaming potentials induced by meteorological effects (Caigniard, 1956; Corwin and Hoover, 1979).

The apparent TE was much larger on surveys run on two low hills, 2495 and 2450, at the southwest and southeast corners of the flank of Crater Peak, respectively. Although the height of the two hills is only 150-250 ft., the TE was about 3700 mV/100 m.

Results

The S-P data were corrected for drift or non-zero traverse ties and are contoured at 100 mV intervals in Figure 4-1. The base line (zero contour) is arbitrary. The heavier contour lines represent topography at 500 ft. intervals.

There are several interesting features. At the top a single traverse starting at 5800 ft. elevation is very positive (+1450 mV). The upper point is 400 ft. in elevation and 2500 ft. horizontally away from the hot lake and fumaroles in the crater. The steep positive gradient could result from circulation associated with this obvious heat source.

Near the 3500 ft. contour we found a +641 to -815 mV dipole anomaly, with 800 ft. separation + to - peak. We would need more data in the area to fully define the anomaly, as there is a 2000 ft. gap between the present lines defining the anomaly and the next east-west line at about 4500 ft. elevation. Using a rough rule-of-thumb to estimate the depth of the source of the anomaly as one half the + to - peak separation, we would find 400 ft or 122 m depth, which may be ±100% (Telford et al., 1976). Some geothermal areas with circulation up along a fault have a dipolar signature in the S-P data (Corwin and Hoover, 1979). As discussed later in this chapter, the dipolar anomaly is close to the controlled source audiomagnetotelluric site #14 which gave low and shallow resistivity values.

There are several negative anomalies, one north-northwest and two northeast of the dipole anomaly, the largest a -700 mV about 2500 ft. to the northeast. These may be as significant as the dipole anomaly. Again, a more detailed S-P survey with more traverse lines would be needed to better define the shape of the anomalies. The present suggested size from the contouring would give a similar depth as the dipole.

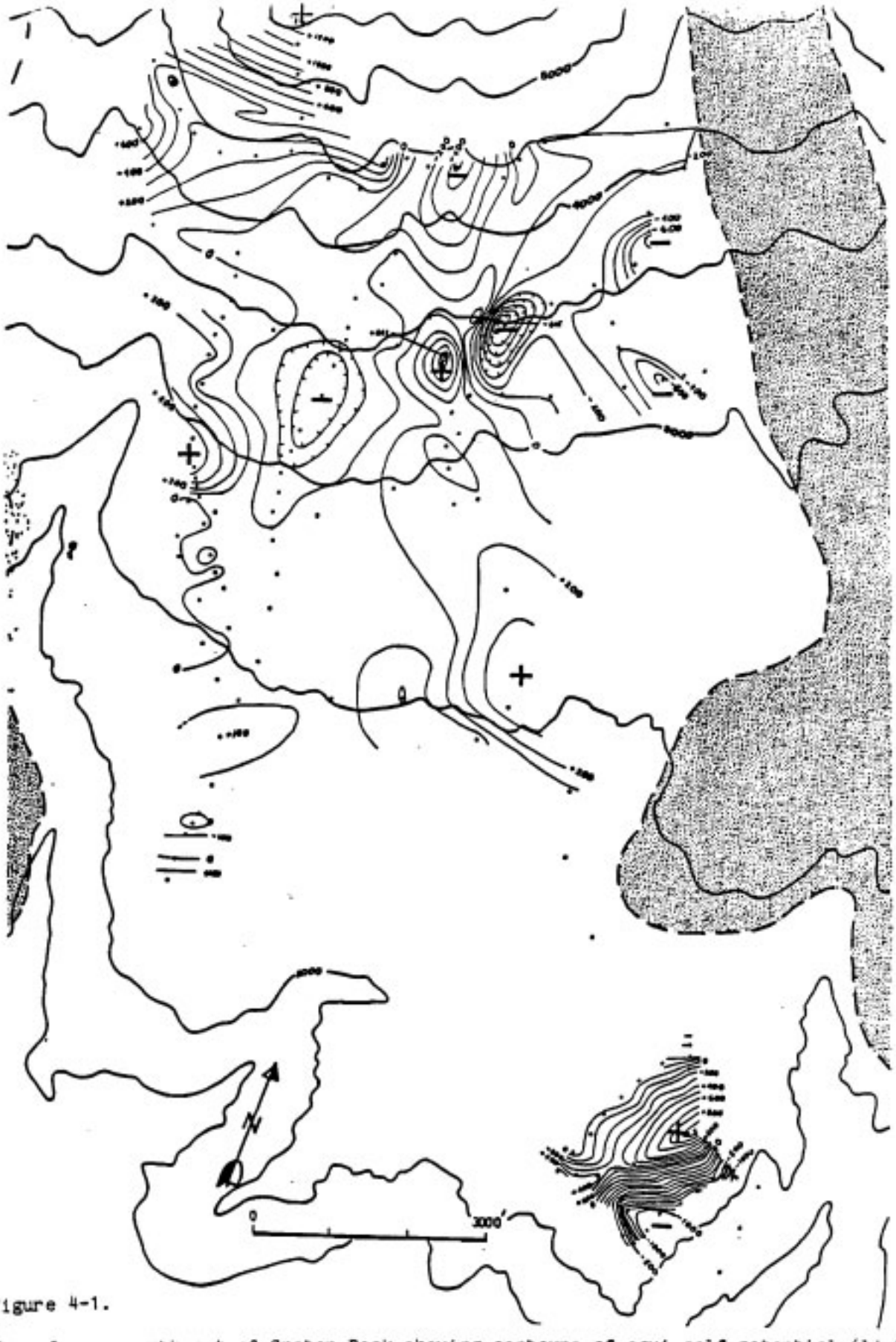


Figure 4-1.

Map of area southeast of Crater Peak showing contours of equi-self-potential (light contours) and topography at 500' intervals (heavy contours). Large + and - signs indicate the polarity of anomalies. Note the linear pattern of two positive and three negative anomalies at about 3500 ft. elevation including a +641 to -815 dipole.

There is a very interesting linear northeast alignment of positive and negative anomalies including the dipole about along the 3500 ft. contour. The hot spring discussed in Chapter 1 lies on the southwest end of that alignment. Another very profound S-P anomaly is located on hill 2450 at the southeast corner of the survey area (Figure 4-1). There is a +1000 mV peak, dropping off to over -1000 mV to the southeast. The significance of this anomaly is somewhat uncertain because of the extreme TE apparent in the data. It is possible that the hydraulic circulation responsible for the TE is complex, and that very high near-surface resistivity amplifies the effect. Yet a 2000 mV anomaly is hard to dismiss offhand. As will be discussed below, the CSAMT resistivity measurement on the hill shows a very low resistivity zone about 1 km beneath the hill.

## DEEP ELECTRICAL RESISTIVITY MEASUREMENTS

### Introduction

The second, deeper method used was the controlled source audiomagnetotelluric (CSAMT) method. Geothermal reservoirs can often be detected by measuring the electrical resistivity vs. depth from the surface. This is due to the fact that the resistivity of geothermal reservoirs is usually significantly lower than the resistivities of surrounding formations. The resistivity tends to be lower for two reasons: 1) resistivity of the water filling the pore spaces of the reservoir rock decreases with increasing temperature, and, 2) the hot water is able to dissolve more minerals than normal temperature ground water.

Explanation of the CSAMT Method

Caigniard (1953) provided the basis for the magnetotelluric method of investigating resistivity vs. depth. Natural variations in the earth's magnetic field called micropulsations cause electric current to flow in the ground. By measuring the magnetic and perpendicular electric fields at the earth's surface at a wide range of frequencies, the apparent resistivity vs. frequency can be calculated: $\rho_a = \frac{1}{5f}\left|\frac{E_x}{H_y}\right|^2$ where $\rho_a$ is the apparent resistivity in Ω-m, f is the frequency in Hertz (cycles per second), $E_x$ is the electric field in mV/km and $H_y$ is the magnetic field variation in gammas. The phase angle $\phi$ between $E_x$ and $H_y$ is also measured to provide a curve of $\phi$ vs. frequency. Caigniard (1953) showed that for an earth approximated by horizontal layers it was possible to interpret the apparent resistivity vs. frequency and phase angle vs. frequency curves in terms of true resistivity vs. depth. The depth of penetration of the magnetic and telluric waves depends upon frequency and resistivity, and is called the skin depth = $503\sqrt{\rho/f}$ (m) or $1650\sqrt{\rho/f}$ (ft) where $\rho$ is the earth's resistivity in Ω-m and f is the frequency in Hz. Table 4-1 shows the skin depth in ft vs. frequency and resistivity.

Table 4-1

Skin Depth in Ft., Resistivity in Ω-m

| f(Hz) | 5 | 10 | 20 | 40 | 80 | 160 | 320 | 640 | 1280 |
|---|---|---|---|---|---|---|---|---|---|
| 256 | 230 | 325 | 462 | 653 | 922 | 1305 | 1843 | 2668 | 3681 |
| 128 | 325 | 462 | 653 | 922 | 1305 | 1843 | 2608 | 3687 | 5218 |
| 64 | 462 | 653 | 922 | 1305 | 1843 | 2608 | 3687 | 5218 | 7377 |
| 32 | 653 | 922 | 1305 | 1843 | 2608 | 3687 | 5218 | 7377 | 10434 |
| 16 | 922 | 1305 | 1843 | 2608 | 3687 | 5218 | 7377 | 10434 | 14757 |
| 8 | 1305 | 1843 | 2608 | 3687 | 5218 | 7377 | 10434 | 14757 | 20867 |
| 4 | 1843 | 2608 | 3687 | 5218 | 7377 | 10434 | 14757 | 20867 | 29513 |
| 2 | 2608 | 3687 | 5218 | 7377 | 10434 | 14757 | 20867 | 29513 | 41738 |
| 1 | 3687 | 5218 | 7377 | 10434 | 14757 | 20867 | 29513 | 41738 | |
| .5 | 5218 | 7377 | 10434 | 14757 | 20867 | 29513 | 41738 | | |
| .25 | 7377 | 10434 | 14757 | 20867 | 29513 | 41738 | | | |
| .125 | 10434 | 14757 | 20867 | 29513 | 41738 | | | | |
| .0625 | 14757 | 20867 | 29513 | 41738 | | | | | |

The frequencies used in Table 4-1 are in the audio range and a little lower. Skin depths of at least 40,000 ft are possible with natural audiomagnetotelluric soundings.

One drawback to the magnetotelluric method is that the natural signals of the earth's field are used, and long recording periods are often necessary to derive good apparent resistivity and phase curves because natural signals are unpredictable in strength and direction. In the controlled-source technique this problem is eliminated by using a grounded electric dipole as a signal source. Goldstein and Strangway (1975) showed that if the grounded dipole current transmitter was at a horizontal distance of greater than three skin depths from the E and H receiver, the conventional magnetotelluric interpretations could be applied.

In the CSAMT technique a single frequency is transmitted until sufficient cycles are received to measure $E_x$ and $H_y$ with satisfactory signal-to-noise ratios. The measurements are repeated at a range of frequencies. The receiver system consists of a pair of non-polarizable electrodes at a dipole spacing "a" oriented parallel to the transmitter dipole to measure $E_x$, and usually an induction coil oriented perpendicular to the transmitter dipole to measure $H_y$.

Some assets of CSAMT measurements are: 1) it is a good buried conductor detector; 2) it has excellent lateral resolution (limited only by the receiver "a" spacing), good depth of penetration and relatively fast survey speed; 3) apparent resistivity and phase are calculated in real time so that results can be seen in the field during the survey; and 4) frequency-domain-type filtering can be used for optimum noise rejection. Some disadvantages are: 1) effects of resistivity anomalies in the vicinity of the transmitter may be seen; 2) effects of transition from the near field (D < 3 skin depths) to the far field (D > 3 skin depths) must be carefully removed from the analysis and; 3) modelling cannot always duplicate field results in intensity and sharpness, especially in the case of buried three-dimensional bodies.

Data from a CSAMT survey may be taken from a series of stations along a line, and simply plotted as apparent resistivity with horizontal distance and with frequency as inverse depth to produce a CSAMT pseudo-section. Although the depth scale is only approximate, it is often possible to interpret structures, pick out conducting zones, and delineate horizontal resistivity changes directly. Bostick (1977) presented an algorithm for inverting the apparent resistivity and phase vs. frequency curves to approximate resistivity vs. depth. His algorithm written as a hand-held calculator program by Campbell (1981) can be used to convert the apparent resistivity-frequency pseudo-

section to an approximate resistivity section. The Bostick-produced sections are only approximate, but offer a better idea of the resistivity structure than the raw pseudo-section, and can be used as a starting point in more sophisticated data reduction programs.

Another method for the inversion of magnetotelluric frequency sounding data is incorporated in Program IMSLPW (Anderson, 1979), of the USGS. This program utilizes a nonlinear least squares sub-program for the inversion of impedance versus frequency to resistivity versus layer depth. The program produces a more refined subsurface model than the Bostick program but the two results should generally coincide. Presently, over half of the twenty-four CSAMT sites have been modelled successfully. When the rest are completed, they will form the basis of a master's thesis. The IMSLPW models agree in general with the Bostick models. Figure 4-2 shows a comparison at site 3. Since the IMSLPW modelling is incomplete, we have used only the Bostick models in the CSAMT resistivity contour profiles.

A third program that can act as a check on IMSLPW or Bostick output is the program EMFIN4 (Anderson, 1977). This program computes the magnetic and electric fields about a finite horizontal electric wire source over stratified ground. By entering our modelled data, consisting of resistivities versus layer depths, we can compare the output of magnetic and electric components to our original impedance data. This can be accomplished by calculating the ratios of electric to magnetic field strengths to find the wave impedances. The calculated wave impedances can be compared to the original impedance data to produce the best fit subsurface model.

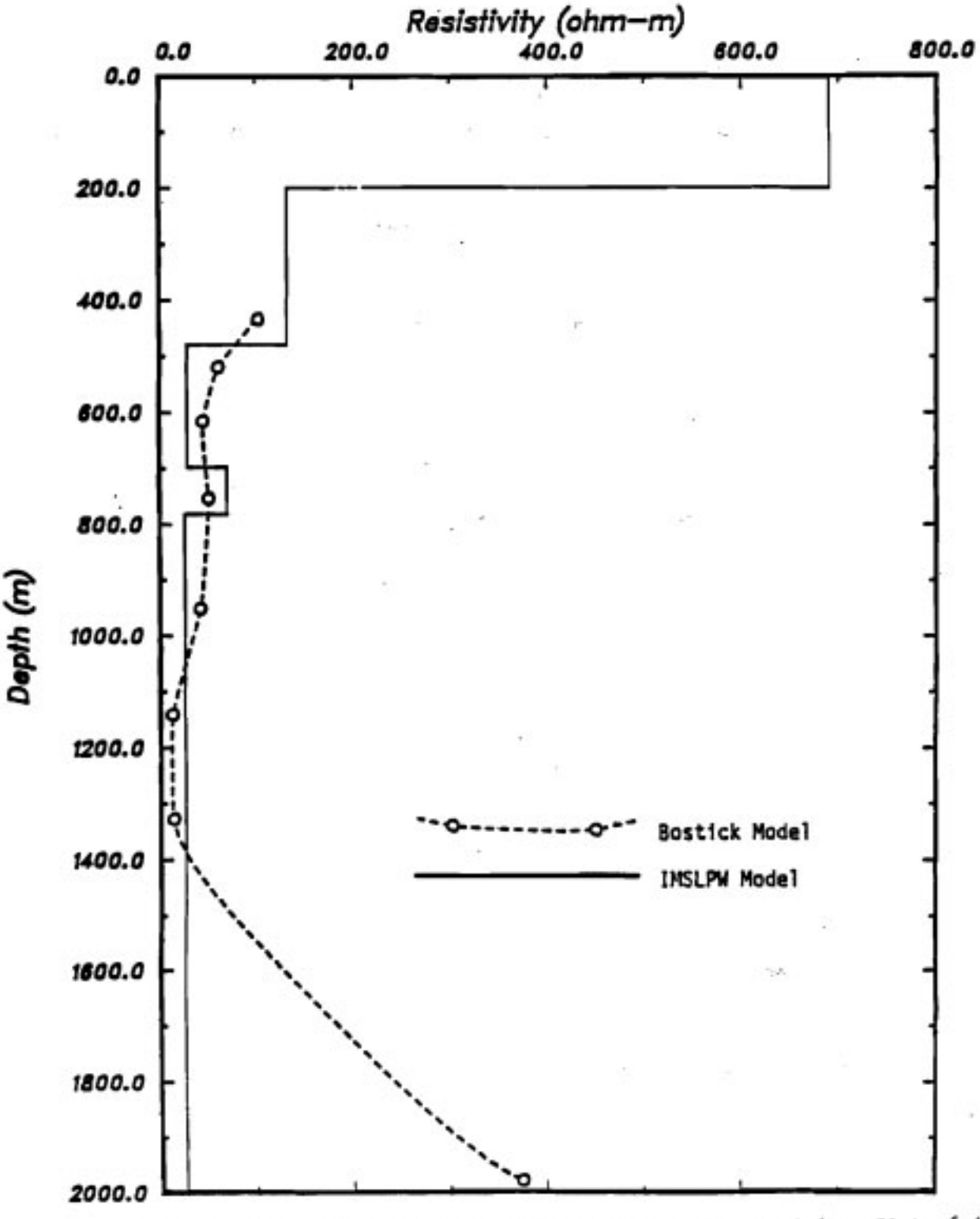


Figure 4-2. Plot of resistivity versus depth for CSAMT site 3 (see Plate 6-1) for two inversion methods.

The CSAMT Survey

The equipment used consisted of a 20 ampere Geotronics FT-20A transmitter powered by a Zonge 30 KVA 400 cycle generator, and controlled by a Zonge Engineering crystal transmitter controller. The $E_x$ and $H_y$ signals were recorded by a Zonge Engineering GDP-12 receiver. The electric field ($E_x$) was measured across grounded dipoles of either 328 ft. (100 m) or 656 ft. (200 m), while the $H_x$ signal was detected with a Zonge high-mu-cored coil of 80,000 turns. The GDP-12 receiver incorporates a computer which converts the analog signals to digital, stacks and averages these signals, and then computes the apparent resistivity and phase angle between E and H. The possible frequencies transmitted are 256, 128, 64, 16, 8, 4, 2, 1, 1/2, 1/4, 1/8, 1/16, 1/32, 1/64 and 1/128 Hz. In our survey we usually only went as high as 64 Hz to conserve the transmitter.

The first transmitting dipole was located on a nearly flat plateau at about 2100 ft. elevation located 4 km northeast of the terminus of Straight Cr. glacier. It was 2.4 km long oriented N20°W (Plate 6-1). Great efforts were taken to achieve low resistance electrode arrays. At each end about 30 metal stakes were driven 3 ft. into the ground. The ground around each stake was saturated with saltwater. A 10 ft. piece of aluminum foil was buried in a trench dug into swampy ground and well salted. Despite these efforts, only 8 amperes could be achieved with the transmitting system. Using this dipole, ten CSAMT stations were measured, ranging from 7 to 13 km distance. Telluric current activity and afternoon thunderstorm sferics necessitated long runs at most low frequencies for sufficient signal stacking.

Nine stations were scattered widely to the east of the canyon separating the camp and the Crater Peak flank where the S-P data were obtained. Station

10 was located just north of hill 2450 with the ±1000 mV anomaly at the southeast end of the S-P survey.

The second CSAMT transmitter dipole was located on a silty river delta in Sec. 7 T13N, R17W, about 10 km west of the Crater Peak survey area. It was 1.8 km long, oriented at N15°W. The saturated silt of the delta provided low contact resistance, and 20 amperes were easily transmitted. Fourteen more sites were occupied, ranging in distance from 4.25 to 18 km from the transmitter. Three sites were occupied in sections 9 and 10 T13N, R17W in the alder flats just east of the Barrier Glacier near where a geothermal lease section was located. Ten sites were on the southeast slope of Crater Peak, and one was a re-occupation of site 4 in the marsh below VABM Chaka.

Except for the last day when station 24 was occupied 18 km from the transmitting dipole, tellurics and sferics proved troublesome, necessitating long stacks and repeats of runs. According to Goldstein and Strangway (1975), the CSAMT method is valid when the transmitter is at least 3 skin depths away from the receiver. In our case, we should have been able to investigate to a skin depth of up to 6 km. However, at all stations there was evidence of a much shallower limit. In theory the phase difference between $E_x$ and $H_y$ should be a positive value between 0 and 90°. As we found in nearly every case, the phase became negative or greater than 90° at frequencies below about 1 Hz. It is likely that this is due to transmitter overprint. When the conductivity structure in the vicinity of the transmitter is appreciably different from the receiver area, this will distort the received E and H. In fact, the geology of both transmitter sites was different from the receiver sites, and probably accounts for the reduced depth limit.

The data were recorded in the field on a Zonge paper printer, then $E_x$ versus f, $H_y$ versus f, $\rho_a$ versus f and $\phi$ versus f were all plotted. From

these plots, spurious values were removed, and the average or best value statistically for multiple runs at one frequency were chosen to result in a smooth curve for inversion to resistivity versus depth. We used an improved Bostick algorithm (Jones and Foster, 1983). The improved transformation which gives a closer approximation to the true resistivity versus depth was programmed on an HP71B for computation of data in the field. Two models of resistivity versus depth are calculated. One uses only the apparent resistivity values and differences between frequencies, the so called $\Delta\rho$ method, and the second uses the apparent resistivity and the phase, the so called $\rho$-$\phi$ method. Usually the two models agree in general with some differences. From the individual plots $\rho(f)$ and $\phi(f)$ we found that the phase was subject to more variations, so we gave more weight to the $\Delta\rho$ models when the two did not agree.

Results

Plate 6-1 shows the twenty-four sample sites. Most of them can be represented along 5 profiles shown in Figures 4-3 to 4-7. Profile A-A' shows the interpreted resistivity versus depth from the rim of Crater Peak to hill 2450 along with the self-potential data on a roughly parallel profile. There is a discontinuous very low resistivity zone (less than 5 Ω-m) under stations 14, 17, 22, 11 and 15. The uphill edge of the zone near station 14 corresponds to the large dipole anomaly in the self-potential data, and the zone under hill 2450 corresponds with the large S-P anomaly there. The low resistivity zone under station 14 is shallow (about 2000 ft.) and nearly the lowest (2.48 Ω-m) of any discovered in the survey. Profile B-B' is nearly perpendicular to A-A' running west from station 14 to 23. The low resistivity zone appears at about

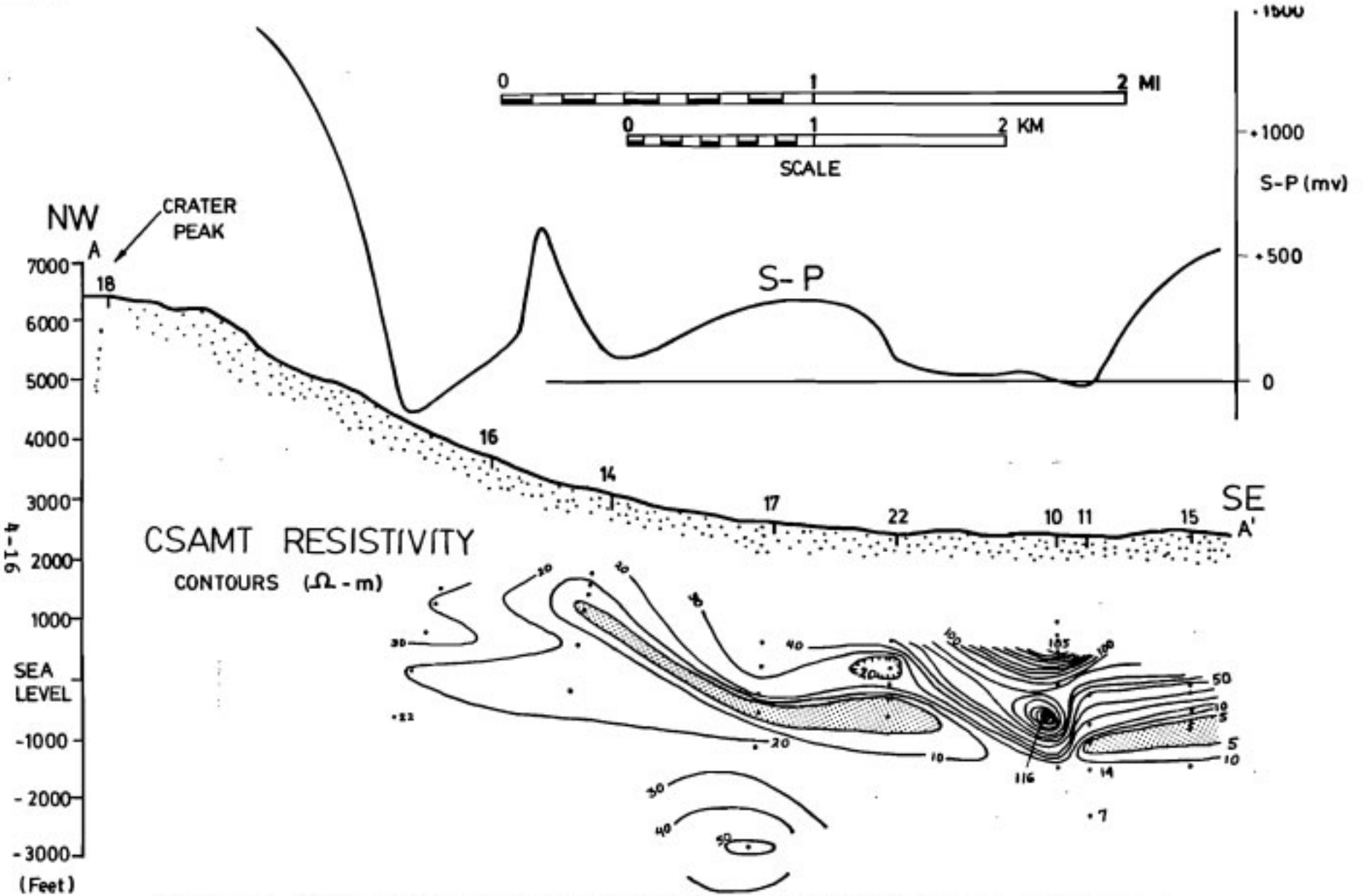


Figure 4-3. Cross section A-A' (see Plate 6-1) showing topography at 1 to 1 scale and contours of equi-resistivity in Ω-m derived from inversion of CSAMT data. Shaded areas show zones of less than 5 Ω-m resistivity. Plotted above the cross section is the S-P profile. The upslope termination of the low resistivity zone corresponds to a large dipole S-P anomaly and a linear pattern of S-P anomalies shown in Figure 4-1.

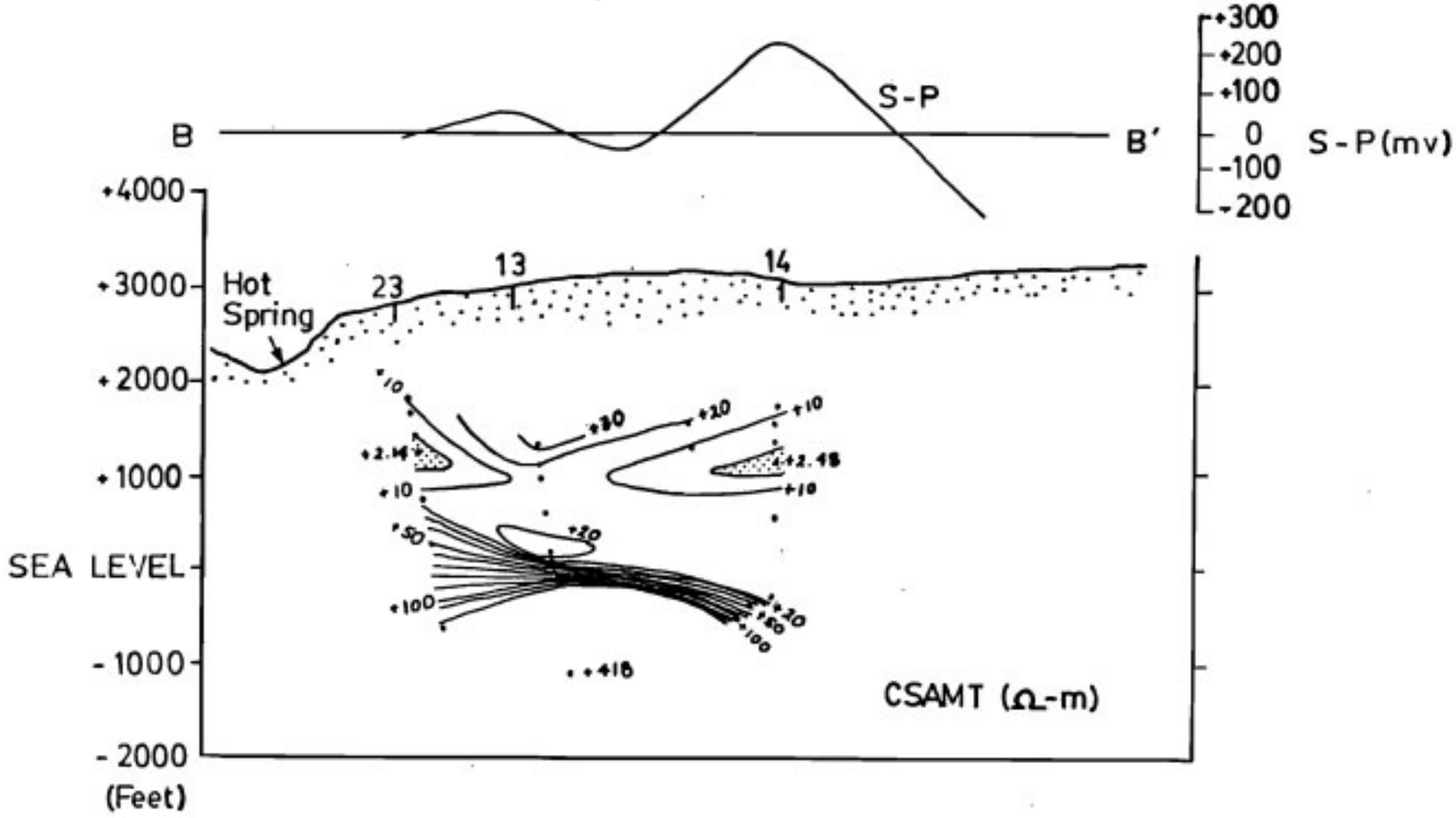


Figure 4-4. Cross section B-B', perpendicular to A-A' (Figure 4-3) showing the low resistivity zone continued to the west along the line of S-P anomalies towards the hot spring.

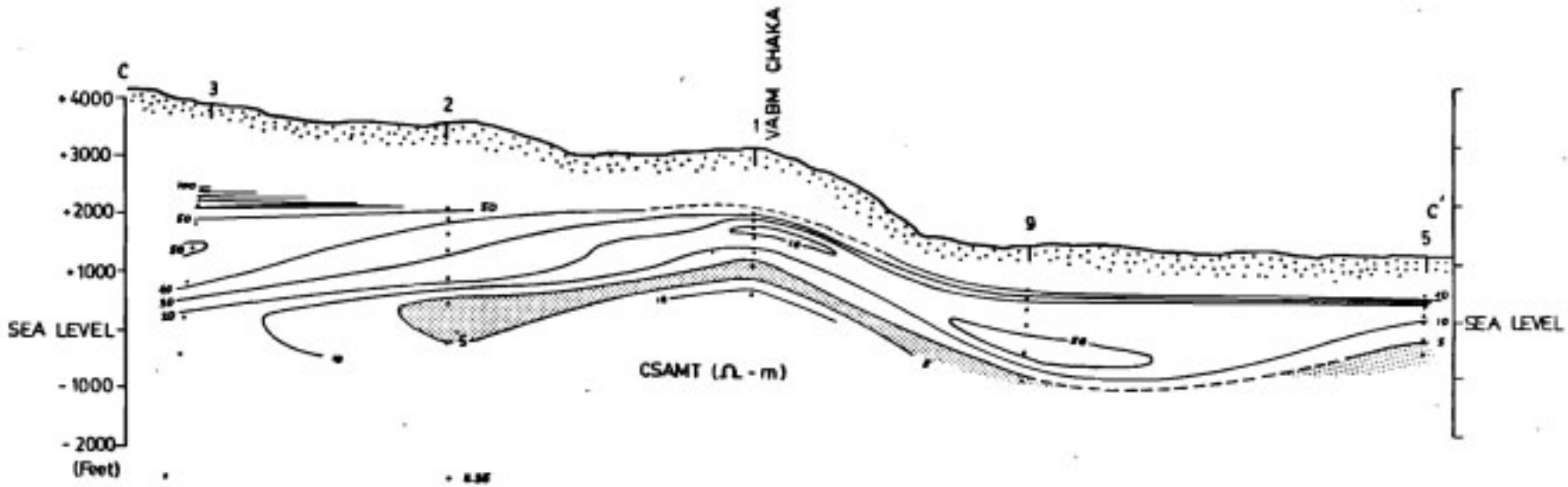


Figure 4-5. Cross section C-C' (see Plate 6-1) showing the topography and CSAMT resistivity data in Ω-m. A low resistivity zone was found beneath stations 2, 1, 9 and 5.

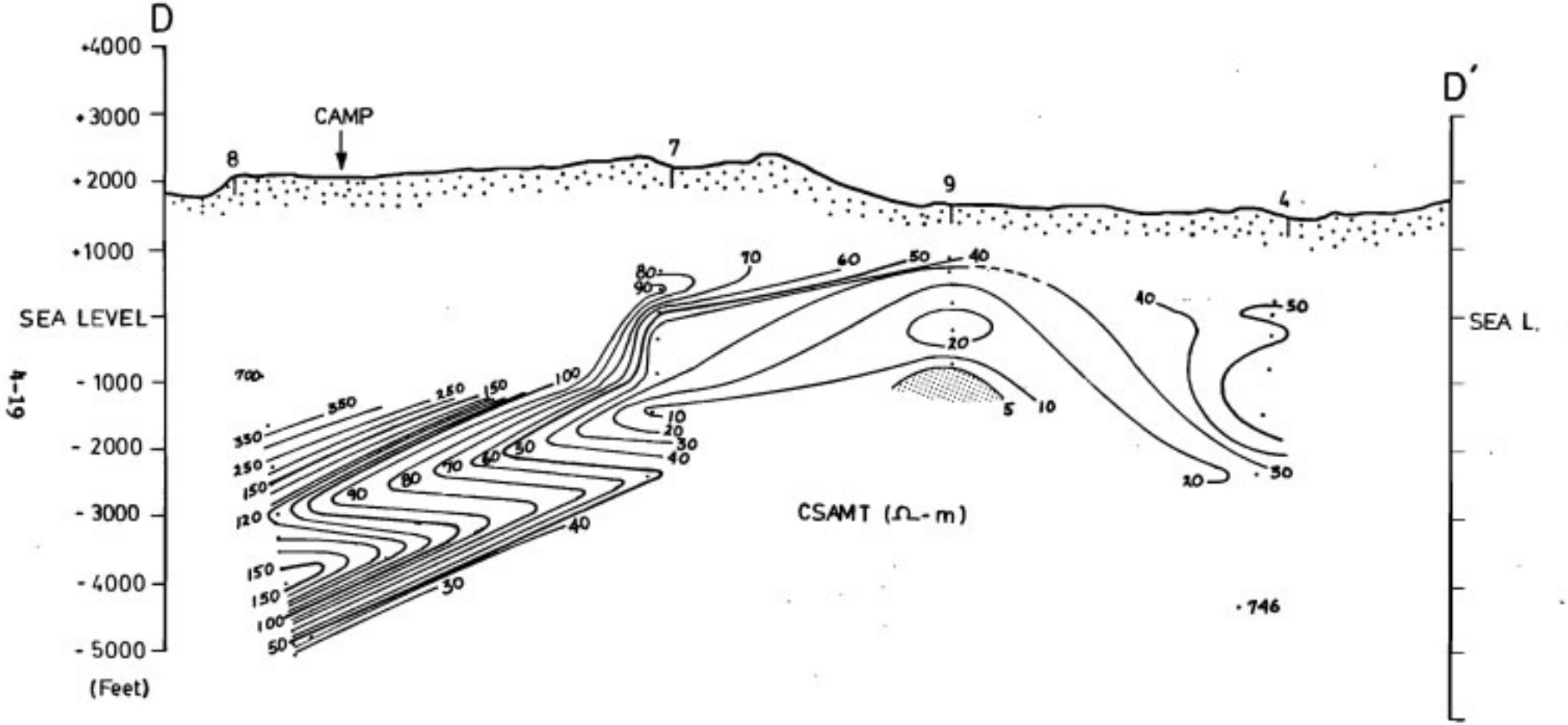


Figure 4-6. Cross section D-D' perpendicular to C-C' (Figure 4-5), showing CSAMT resistivity data in Ω-m. Section C-C' intersects at station 9, indicating the low resistivity zone may be a narrow linear feature.

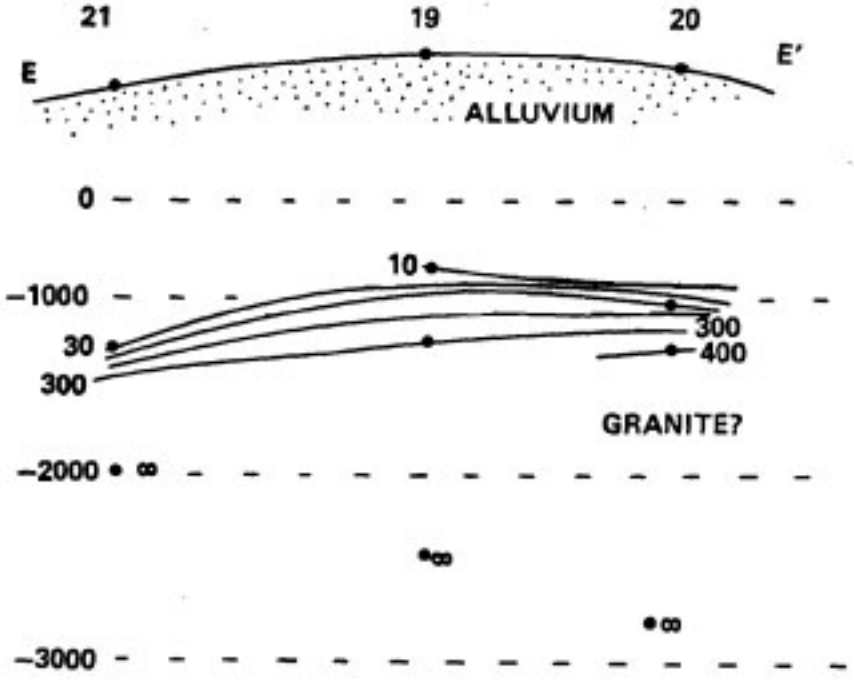


Figure 4-7. Cross section E-E' (see Plate 6-1) showing the CSAMT resistivity data. There is a low resistivity zone over a very high resistivity basement, probably composed of granite.

1650 ft. under station 23 not far from the 40°C hot spring discovered in the canyon. The resistivity increases with depth beneath the low resistivity layer.

Profile C-C', oriented northwest-southeast also shows a discontinuous zone of less than 5 Ω-m at depths ranging from 2360 to 3125 ft. This zone may be fairly narrow as indicated by profile D-D' nearly perpendicular to C-C', where only station 9 and perhaps 7 show the low resistivity zone, but the coverage is insufficient to make a firm conclusion. It is completely absent in data from stations 8 and 4.

Three stations, 19-21, were occupied to the west in sections 9 and 10 and shown as profile E-E' in Figure 4-7. The general character of the CSAMT ρ versus f was quite different in these data compared to those in the rest of the survey. The shallowest data at 64 Hz are fairly low resistivity, 8.5 to 29 Ω-m, but very deep for that frequency, about 2500 ft. At lower frequencies (and depths) the resistivity increased very rapidly to essentially infinity. The great depth at 64 Hz implies high resistivity from the surface on down to some depth less than 2500 ft. where the resistivity is much lower. Within a few hundred feet below the low resistivity zone there is a contact with very much higher resistivity material. As the mountains to the immediate south of the Chakachatna River are granite, we suggest that the basement rocks under profile E-E' are also granite (Plate 1-1). The high resistivity from the surface down is alluvium from south-flowing streams and the Chakachatna River, but whether this accounts for the full 2500' cannot be determined.

## Conclusions

The two electrical methods used, self-potential and CSAMT have revealed some significant anomalies. By necessity, both were conducted as reconnaissance surveys to locate areas of interest, which could be explored in much more detail if warranted.

The CSAMT data have revealed a discontinuous, very low resistivity layer on the southeast flank of Crater Peak. It has a slope roughly parallel to that projected for the ancestral Spurr stratocone. Its upslope termination near station 14 corresponds to a large S-P dipole anomaly. The S-P data show an interesting northeast alignment of anomalies at about the 3500 ft. level coincident with the upslope termination of the low resistivity zone and with the upslope termination of helium anomalies discussed in Chapter 5. The 40°C hot spring in the canyon at the west side of the area is on the extension of the line of S-P anomalies.

The large S-P anomaly under hill 2450 is also underlain by a low resistivity zone of less than 1 Ω-m resistivity. A perhaps narrow low resistivity zone underlies stations 1, 2, 9 and 5 in section C-C'. No S-P surveying was done in that area.

Figure 4-8 presents the CSAMT profiles as a fence diagram to show the relationship of the low resistivity zones to the topography and to each other. There are no data between the two southeast-trending profiles AA' and CC'. So it is quite possible that the two low resistivity zones are connected. The possible sources of this zone are discussed in Chapter 6.

In Chapter 6 we have compared all the evidence, including the electrical geophysical, the helium and mercury soil survey and the geological to suggest prime areas for geothermal energy resources.

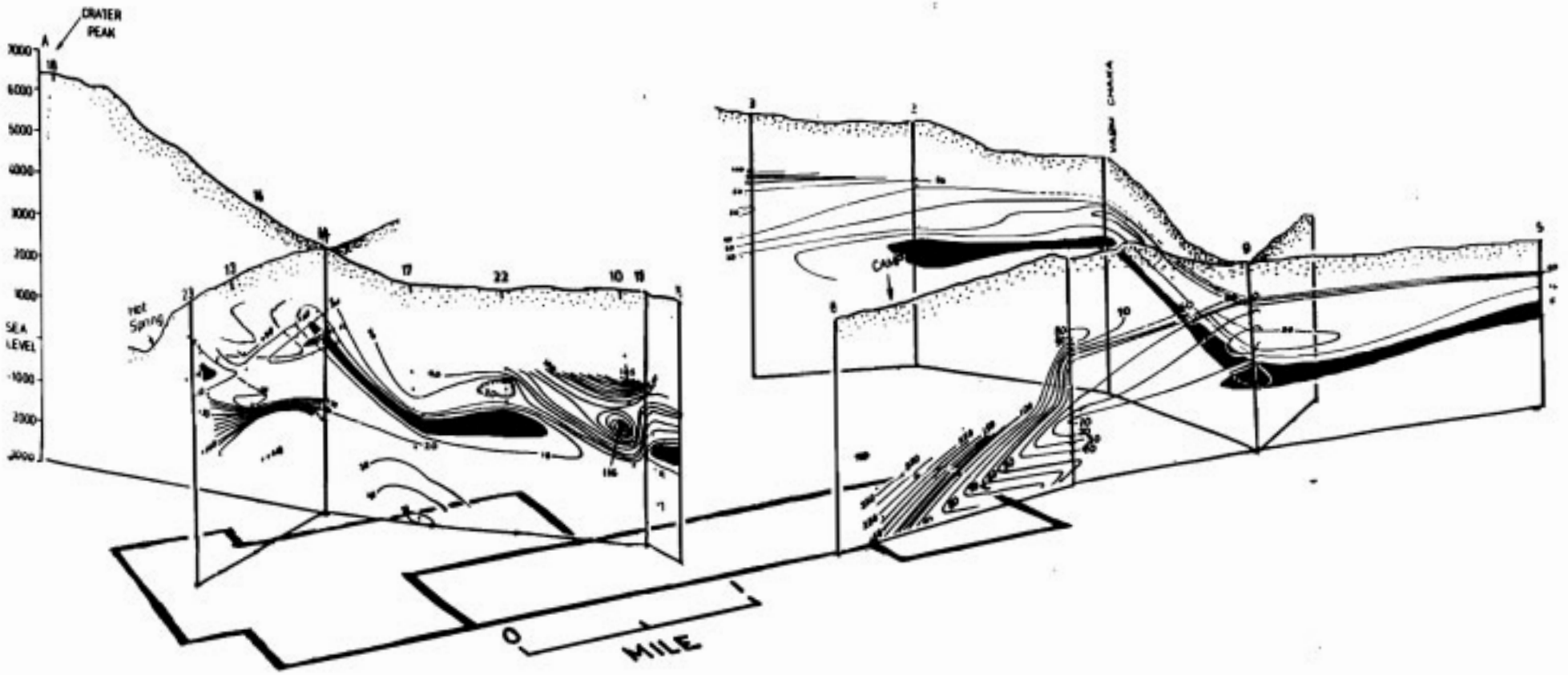


Figure 4-8. Three-dimensional, one-to-one-scale fence diagram of the CSAMT contoured resistivity values of profiles AA', BB', CC', and DD'. The zone of very low resistivity (less than 5 Ω-m) is shown in black. The State geothermal lease block boundaries are also shown. Base line is -3000 ft. elevation. See Plate 6-1 for locations of profiles and lease blocks on a topographic base map.

REFERENCES

Anderson, Walter L., 1977, Electromagnetic fields about a finite electric wire source, Computer Program, National Technical Information Service Report PB-238-199, 205 pp.

Anderson, Walter L., 1979, Inversion of MT/AMT plane wave frequency soundings, Computer Program, USGS Open-File Report 79-586, 37 pp.

Bostick, F. X., 1977, A simple almost exact method of MT analysis, in Ward, S. H., ed., Workshop on Electrical Methods in Geothermal Exploration: Univ. of Utah, Salt Lake City, UT, 84112, p. 175-183.

Caigniard, L., 1953, Basic theory of the magneto-telluric method of geophysical prospecting, Geophysics 18(3), p. 605-635.

Caigniard, L., 1956, Electricité tellurique, in Encyclopedia of physics XLVII, Geophysics I: Springer.

Campbell, D. L., 1981, MT inversion (Bostick's Algorithm) calculator program EM-8. In: Manual of Geophysical Hand-Calculator Programs, Society of Exploration Geophysicists, HP Volume, p. 1-8.

Corwin, R. F. and D. B. Hoover, 1979, The self potential method in geothermal exploration, Geophysics, 44, 226-245.

Ernstson, K. and H. Ulrich Scherer, 1986, Self-potential variations with time and their relation to hydrogeologic and meteorological parameters, Geophysics 51(10), 1967-1977.

Goldstein, M. A. and D. W. Strangway, 1975, Audio-frequency magnetotellurics with a grounded electric dipole source, Geophysics Vol. 40 (4), p. 699-683.

Jones, A. G. and J. H. Foster, 1983, An objective real-time data adaptive technique for efficient in-field model resolution improvement in magneto-telluric studies, extended abstract of paper presented at 1983 Society of Exploration Geophysics meeting, Las Vegas.

Morrison, H. F., R. F. Corwin, G. de Moully and D. Durand, 1978, Semi-annual technical progress report, contract 14-08-0001-16546, Univ. of California, Berkeley.

Republic Geothermal, 1983, Unalaska Geothermal Project, Phase 1B Final Report for the Alaska Power Authority, 1:67-70.

Telford, W. M., L. P. Geldart, R. E. Sheriff and D. A. Keys, 1976, Applied Geophysics, Cambridge University Press, New York, 458-466.

Zabloski, C. J., 1976, Mapping thermal anomalies on an active volcano by the self-potential method, Kilauea, Hawaii, Proc. 2nd U.N. Symposium on Development and Use of Geothermal Resources, San Francisco, CA, U.S. Government Printing Office, Washington DC 2:1299-1309.

Chapter 5

# Mercury and Helium Soil Surveys at Mt. Spurr, Alaska

by

Donald L. Turner, Eugene M. Wescott and David Bratt

## MERCURY SURVEY

### Introduction

Mercury (Hg) is a highly volatile element found in most rocks in small concentrations. Its high vapor pressure makes it extremely mobile, and the elevated temperatures near a geothermal reservoir increase this mobility. During the rise of geothermal hot water from deep levels, a vapor phase (normally $CO_2$-rich) will start to exolve and Hg will partition into this vapor phase (Varekamp and Busek, 1983). Therefore, an Hg aureole develops above the zone of rising hot water. Such aureoles are typically much larger in area than a corresponding helium anomaly. Volatilized Hg is extremely mobile, and is known to have penetrated at least several hundred meters (about 1000 ft) of rock overlying base metal ore deposits (McNerney and Buseck, 1975).

Mercury content in soils has been reported as a geothermal resource indicator by several workers. Matlick and Buseck (1975) confirmed a strong association of mercury with geothermal activity in three of four areas tested (Long Valley, California; Summer Lake and Klamath Falls, Oregon). Using the Hg concentrations in the A horizon of soils on a 1.6 km spacing interval, they

found broad Hg anomalies outlining the geothermal areas. Phelps and Buseck (1978) also found broad Hg soil anomalies in two other geothermal areas, Yellowstone and Coso Springs, California. Capuano and Bamford (1978) used close-spaced traverses across the Roosevelt Hot Springs, Utah, Known Geothermal Resource Area (KGRA) to define structures controlling fluid flow and to delineate areas of near-surface thermal activity. Landress and Klusman (1977) also confirmed that anomalous Hg concentrations were found in A and B soil horizons in geothermal areas. Wescott et al. (1981) found very good correlation between soil Hg and elevated ground temperatures at Chena Hot Springs, Alaska. Wescott (1981) also investigated soil Hg content vs ground temperature at 4.5 m depth at the Pilgrim Springs, Alaska KGRA. East (1982) found good correlation between elevated temperatures and soil Hg at Manley Hot Springs, Alaska. Republic Geothermal, 1983, used anomalous Hg concentrations in the B-1 soil horizon on Unalaska Island, Alaska to successfully site a geothermal well. These results show that mercury soil surveys are a very useful technique for geothermal exploration.

Fang (1978) has shown that mercury can be captured by adsorption on clay minerals, by adsorption on iron and manganese oxides and by reactions with organic materials. The process of Hg soil enrichment is a dynamic process. Revolatilization and biogenic uptake with subsequent volatilization will remove Hg from the soil continuously. A steady-state system will be present after an initial period of non-equilibrium (Varenkamp and Busek, 1983). This process of continuous Hg loss has enabled these workers to distinguish between areas of old and current hydrothermal activity. They have documented several cases where zones of fossil hot spring activity lack Hg enrichments, whereas active zones are enriched in Hg. They have concluded that adsorbed or organically bound Hg will be lost to the atmosphere, possibly within a few decades after the cessation of hydrothermal activity.

Sampling and Analytical Methods

Geothermal Hg is usually concentrated in one or more of the soil profile layers. The optimum depth of soil sampling is usually determined by collecting and analyzing soils from three different soil horizons (A-3, B-1, C-1) at the same location (Republic Geothermal, 1983). Republic geologists found that the B-1 layer was the best sampling horizon on Makushin Volcano, Alaska. The A-3 soil horizon contains an organic-rich material which causes analytical interference and, on Makushin, the C-1 horizon occurrs at unreasonable sampling depths (greater than 3 feet).

It was not possible to sample a uniform soil horizon in the Mt. Spurr survey, due to the numerous tephra deposits that blanket the area. However, thin soils were developed in some areas and these were sampled where possible. Our sampling procedure was to dig a 2-foot pit with a shovel and to sample the deepest soil level present. If no soil layer was present, a tephra sample was collected from the 2-foot depth. We were initially concerned about possible sampling bias caused by this technique. In order to evaluate this possible sampling problem, we plotted all measured Hg values against sample depth. This plot showed no correlation, suggesting that variable sampling depth did not cause a significant sampling bias.

Individual samples were collected in ziplock plastic bags, dried on paper towels in the shade, and sieved to <80 mesh size. The <80 mesh samples were then stored in sealed glass vials until analyzed. All samples were analyzed with a Jerome Instruments model 301 mercury detector which uses a thin gold film technique. This instrument has a sensitivity of one part per billion (ppb). The instrument was calibrated with known volumes of air saturated with Hg vapor at measured ambient temperature.

Results of the Mt. Spurr Mercury Survey

Two hundred and two soil and tephra samples were taken at 189 stations on the south side of Mt. Spurr, primarily in the accessible areas above the extensive alder cover. The flanks of Crater Peak were sampled intensively. Preliminary analyses were performed in the field and the presence of anomalously high Hg values was initially used to direct other survey activities. All samples were later analyzed in the laboratory using the same instrument. Values ranged from essentially zero to 159 ppb, except at the Crater Peak fumarole field, where extremely high values exceeding the upper measurement limits of the instrument were found.

There is no "standard" background value for soil mercury. An appropriate background value must be determined for each survey area based on widespread sample measurements. Figure 5-1 is a histogram of the mercury values. The mode of these values is 4 ppb and background was estimated to be 5 ppb. Plate 5-1 shows the map distribution of mercury values plotted as 2, 4, 8 and 16 times background. Except for samples at Crater Peak and near the Mt. Spurr summit, all of the highest values (>8 x background) are located on the tephra apron that forms the south slope of Crater Peak. Numerous background and relatively low-level samples are also located in this same area (Plate 5-1), indicating that the entire tephra blanket is not uniformly high in mercury.

The presence of extremely high values (off-scale on our instrument) at the Crater Peak fumarole field, together with a value of 159 ppb from a tephra sample at the south rim of Crater Peak (highest non-fumarole value measured in the survey), indicate that the Crater Peak vent is presently a major source of mercury. This might be considered to cause a serious problem for the interpretation of our survey results in that a significant number of the high

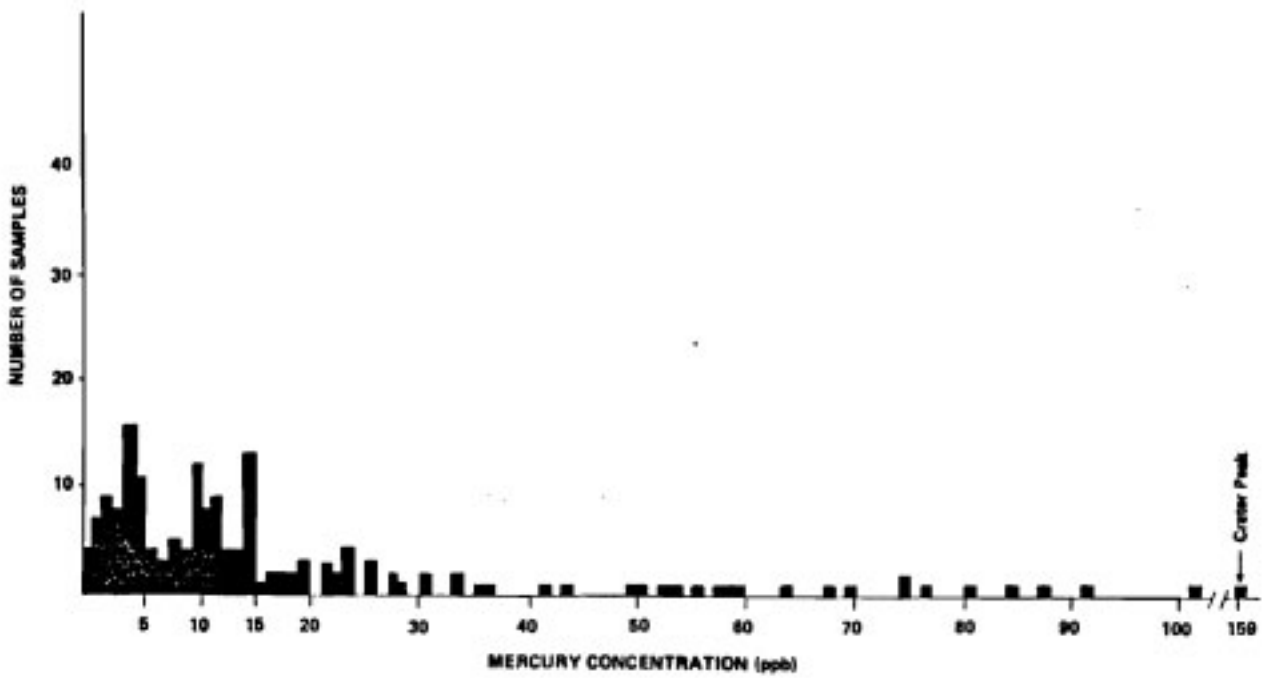


Figure 5-1. Histogram of mercury values.

mercury values in the area could possibly represent high Hg content tephras deposited by Crater Peak eruptions. If so, these values would not be valid indicators of Hg rising to the surface above a geothermal heat source located below the sample locality. However, the expected temperatures for basaltic tephra-forming eruptions are on the order of 800-1200°C, and any mercury present during an eruption would certainly be volatilized at much lower temperatures than these.

The fact that other geothermal indicators (helium, self-potential and CSAMT anomalies discussed in subsequent sections) are also present in the same area together with numerous background Hg values, suggests that the mercury anomalies are caused by geothermal sources at depth.

## HELIUM SURVEY

### Characteristics and Sources of Helium

An extensive discussion of helium surveying as a geothermal exploration method is given in Wescott and Turner (1985). Accordingly, only a brief review of the method is given in this report.

Helium is the second lightest known element with a density of 0.1381 grams/liter (hydrogen is 0.0695 and air is 1). It has a molecular and atomic weight of 4 and is an inert, elemental gas with no known chemical compounds. Helium's low solubility in cold water, monatomic molecular structure, low cross-section capture coefficient, extremely light weight, chemical inertness and high diffusivity give it a unique advantage over other geochemical trace elements in that helium will always migrate from its source to the surface of the earth.

Helium is steadily generated by radioactive elements in rocks and minerals. This occurs when alpha particles (released by decay in the uranium and thorium isotope series) capture two electrons to form atoms of inert helium. Other sources of helium on earth, such as those due to primordial accumulations, cosmic radiation, meteorites, radioactive tritium decay, etc., do not contribute significantly to the total annual production.

Helium production differs considerably in different rock types due to variable uranium and thorium content. Helium loss to the atmosphere is only about five percent of its rate of production, indicating that most of the helium produced is trapped within the earth in various ways. Helium movement through the geologic column is a complex combination of fluid transport and gaseous diffusion. Studies have shown that the distance helium moves by diffusion is several orders of magnitude smaller than the distance moved in equal time by fluid transport.

Helium is very unusual in that its solubility in water increases with temperature above 30°C (Mazor, 1972). In a geothermal system, pressurized hot water will therefore be a very efficient scavenger of helium produced by radioactive decay of uranium and thorium contained in the rocks at depth. This scavenged helium will be released as the heated water rises towards the surface, cools and depressurizes. Since helium is highly mobile it will seek faults, fractures and pore spaces to rise to the surface above the geothermal system. The ability of helium to migrate away from its ultimate source of radioactive rocks and to accompany geothermal systems provides a convenient geochemical tracer. In fact, it appears that helium might even be considered a direct indicator for geothermal reservoirs since elevated levels of helium are observed at most geothermal sites.

Exploration Techniques

Helium surveys have been developed and perfected as a time-and-cost-effective geothermal exploration method. The ability of helium to migrate long distances through the geologic column creates anomalies which can be defined by water, soil and soil gas sampling. Helium surveys provide a rapid sampling technique that can be used with minimum effort and at relatively low cost. Samples can be collected as water, soil or soil gas and then analyzed for helium to better than 10 parts per billion in the gaseous sample by mass spectrometry. It is this precise analytical capability that only recently has permitted helium to be utilized as an effective trace element in geothermal exploration.

Due to helium's ability to escape from a geothermal system at depth, anomalies will be noted above fractures connected to the geothermal reservoir. In some cases this may be the only identifiable geochemical indicator, since precipitated calcite and silica may have effectively sealed the reservoir and prevented heavier elements from reaching the surface. Although there may be an active reservoir at depth, near-surface temperature anomalies may be slight or even nonexistent. Positive temperature anomalies will usually coincide with helium anomalies, although there may be some offset. This is a very significant correlation and gives the geothermal explorationist an additional method with which to define optimum drill sites for reservoir confirmation.

Regional helium surveys generally require a sample density of one to five samples per square mile. Detailed exploration is usually conducted with a 0.1 mile grid spacing, which can be followed up with sample spacing of 50 to 100 ft in the most anomalous zones. If an elongate reservoir is expected (such as a rift or parallel fault/fracture zone) the grid can be modified accordingly.

## Sampling Methods and Analytical Procedures

Figure 5-2 (after Pogorski and Quirt, 1981) illustrates how helium occurs in soil, and indicates various ways it can be sampled. We sampled the soil and tephra layers in the Mt. Spurr area by digging a 2-ft pit with a shovel, collecting the lowest exposed soil or silt-to-sand size tephra layer from the side of the pit, removing any pebbles or larger size rock fragments, and hermetically sealing the sample in a special aluminum container. The station barometric pressure, air and soil temperatures and sample depth were recorded at each station. The samples were shipped to Chemical Projects Ltd., Toronto, Canada, for mass spectrometric analysis of helium and hydrocarbon gasses.

## Helium Survey Results

Fifty-seven samples were collected. A full report and a preliminary interpretation of all analytical results are given in the report produced by Chemical Projects Ltd. which is included as Appendix A to this report. In this chapter we will address only the main results and interpretation of this work.

The sample population can be divided into three groups:

Group 1 - 40 soil samples (samples in which the micropores contain a gas phase)

Group 2 - 16 mud samples (soil samples in which the micropores are completely filled with water)

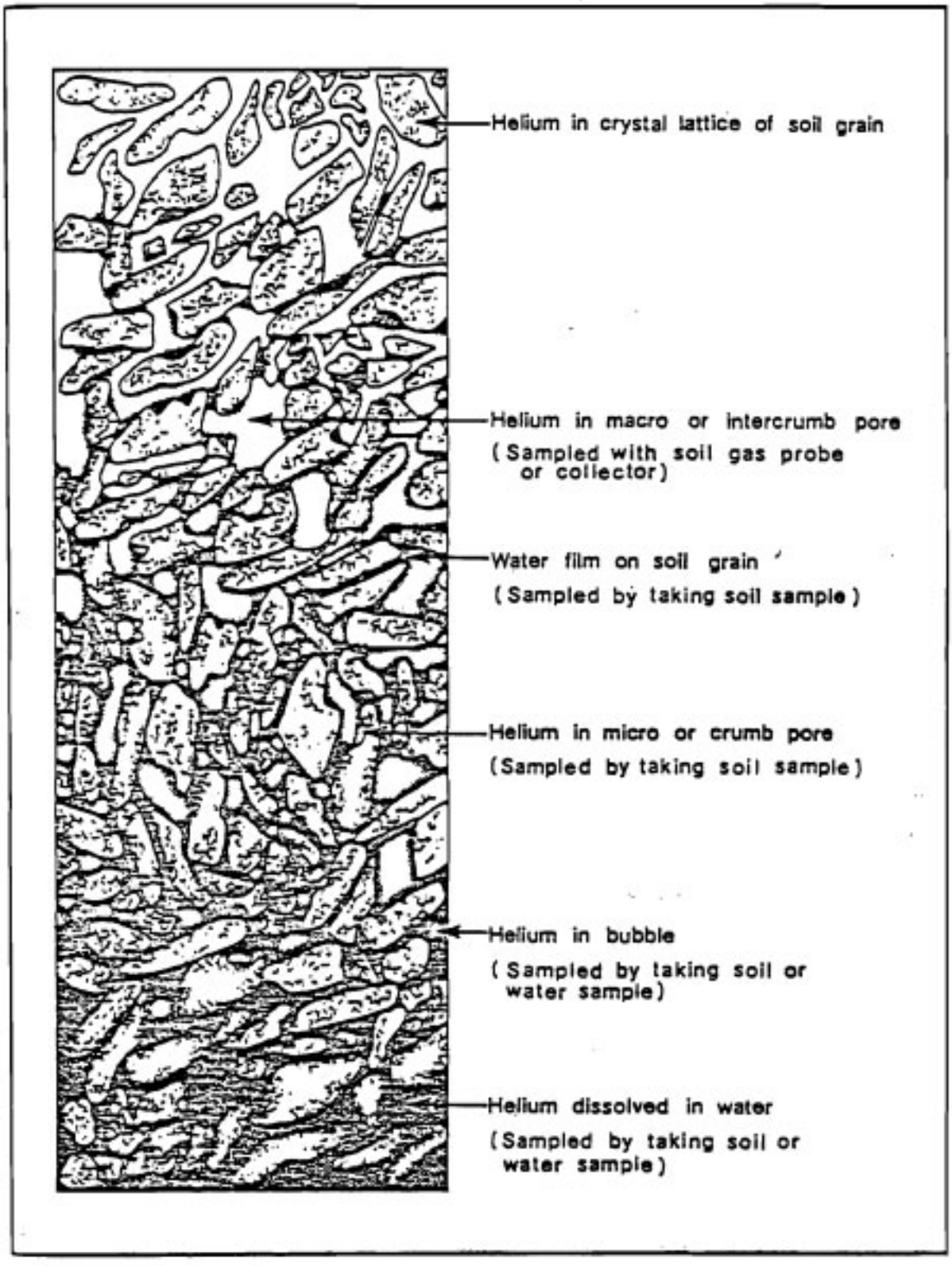


Figure 5-2. Schematic diagram showing how helium occurs in soil. From Pogorski and Quirt (1981).

Group 3 - 1 water sample (a sample of water collected from a free-flowing warm spring)

The first two groups of samples have been treated statistically as separate groups. Each of these two groups has its characteristic range of helium and hydrocarbon values. The individual helium and hydrocarbon values are comparable within each specific group but not outside of a given group. In order to compare helium levels in soil and mud, the data are presented on Plate 5-2 in terms of standard deviations above the background mean.

The mean value of helium in the background population is 5.47 ppm for the soil samples and 9.42 ppm for the mud samples. These values are slightly higher than normal helium background levels. The higher background values indicate that the sampling grid was not large enough to fully extend beyond the anomalous areas. The range of helium values in the soil samples varies from 1.37 to 12.8 ppm and in the mud samples from 6.66 to 39.5 ppm. The mean background value of methane is 117.5 units (cc gas at NTP/gram of soil) for the soil samples and 9.42 units for the mud samples. The range of methane values in the soil samples varies from 60 to 4440 units and in the mud samples from 2 to 931 units. These methane values are within the range of methane levels which can be generated close to the surface by biogenic activity (Pogorski, Appendix A).

A number of samples contain low concentrations of hydrocarbons of the $C_2$ and $C_3$ series. The two lowest values of helium observed (1.37 and 3.51 ppm) are probably due to the depressing effect of hydrocarbon emanations in the ground. It is likely that these emanations exceed the rate of the helium flux at the above stations. The water sample collected from the warm spring in the valley below Crater Peak has a low helium value (4.12 ppm) and a low methane

value of 34 units. This low helium value may have resulted either from helium and hydrocarbons escaping prior to sample collection or because the water flow rate was greater than the helium emanation rate (Pogorski, Appendix A).

Plate 5-2 shows a general concentration of anomalously high helium values on the south slope of Crater Peak, several scattered high values to the east, and one high value about 4 km west of the Crater Peak south slope anomaly area. With very few exceptions, high helium values are coincident with high mercury values (Plate 5-1), lending support to the hypothesis that these coincident anomalies have a geothermal source.

We wish to draw particular attention to the NE-trending boundary formed by the northernmost anomalous helium values located on the south slope of Crater Peak. Northwest of this "line" all helium values are less than 1 standard deviation above background. The boundary line occurs near the major slope break of the Crater Peak cone. This boundary line also appears to be related to significant features found in our self-potential and CSAMT surveys discussed in Chapter 4. The juxtaposition of all of these different types of anomalies and their significance for geothermal resource assessment will be discussed in Chapter 6.

## REFERENCES

Capuano, R. M. and R. W. Bamford, 1978, Initial investigations of soil mercury geochemistry as an aid to drill site selection in geothermal systems: University of Utah Research Institute, Earth Science Laboratory Report IDO/78-1701-b. 3.3, 32 p.

East, J. 1982, Preliminary geothermal investigations at Manley Hot Springs, Alaska, Geophysical Institute, University of Alaska Report UAG R-290, p. 52-55.

Fang, S. C., 1978, Sorption and transformation of Hg vapour by dry soil, Environmental Science and Technology, v. 12, p. 285-288.

Landress, R. A. and R. W. Klusman, 1977, Nature of the occurrence of mercury in soils of geothermal areas: Georgia School of Mines, Dept. of Chem. and Geochem. Final Report, U.S. Geol. Survey Grant No. 14-08-001-G-335, p. 116.

Matlick, J. S., III and P. R. Buseck, 1975, Exploration for geothermal areas using mercury: a new geochemical technique, In: Proc. Second United Nations Symposium on the Development and Use of Geothermal Resources, v. 1, p. 785-792.

Mazor, E., 1972, Paleotemperatures and other hydrological parameters deduced from noble gases dissolved in groundwaters; Jordan Rift Valley, Israel: Geochimica et Cosmochimica Acta, v. 36, p. 1321-1336.

McNerney, J. J. and P. R. Buseck, 1975, Geochemical exploration using mercury vapor, Economic Geology, v. 68, p. 1313-1320.

Phelps, D. W. and P. R. Buseck, 1978, Natural concentrations of Hg in the Yellowstone and Coso geothermal fields: Geothermal Resources Council, Transactions, v. 2, p. 521-522.

Pogorski, L. A. and G. S. Quirt, 1981, Helium emanometry for hydrocarbons, part I, in unconventional techniques in exploration for petroleum and natural gas, Southern University Press, Dallas, Texas, pp. 124-135.

Republic Geothermal, 1983, Unalaska geothermal project, phase 1B, Final Report Vol. 1 for the Alaska Power Authority, p. 29-36.

Varekamp, J. C. and P. R. Busek, 1983, Hg anomalies in soils: a geochemical exploration method for geothermal areas, Geothermics, v. 12, no. 1, p. 29-47.

Wescott, E. M., 1981, Helium and mercury in the central Seward Peninsula rift system, Alaska, In: Geothermal Reconnaissance Survey of the Central Seward Peninsula, Alaska, E. M. Wescott and D. L. Turner, eds., Geophysical Institute, University of Alaska Report UAG R-284, p. 37-59.

Wescott, E. M. and D. L. Turner (eds.), 1985, Geothermal energy resource investigations in the Eastern Copper River Basin, Alaska, Geophysical Institute, University of Alaska Report UAG R-302, 158 pp., 8 plates.

Wescott, E. M., W. Witte, A. Dunn and A. Lockhart, 1981. Helium and mercury soil sampling, In: A Geological and Geophysical Study of the Chena Hot Springs Geothermal Area, Alaska, Geophysical Institute, University of Alaska Report UAG R-283, p. 54-61.

Chapter 6

# Summary and Conclusions of the Mt. Spurr, Alaska, Geothermal Energy Assessment Project

by

Donald L. Turner and Eugene M. Wescott

Spurr volcano is a composite Quaternary cone of largely andesitic composition located on the west side of Cook Inlet about 80 miles west of Anchorage and about 40 miles from the Beluga electrical transmission line (Figure 1-1). The south side of the Spurr cone has been breached. A small, Holocene, composite cone, Crater Peak, occupies the breach (Figure 1-2). The upper part of the original volcano is no longer present. The upper part of the mountain is a 4.5 km-diameter, snow-and-ice-filled basin, believed by some previous workers to possibly represent a caldera (Figure 1-2). Our VLF resistivity surveys indicate that snow-and-ice depth exceeds 500 m in the deepest parts of the basin, a finding that is consistent with the idea that the top of the original volcano has collapsed. The center of this summit depression is occupied by the small, Holocene, summit cone of Mt. Spurr.

K-Ar dating indicates that much of the ancestral Spurr volcano was built between about 250,000 and 60,000 years ago. Geologic mapping does not support the caldera hypothesis, but, instead, indicates that a Mt. St. Helens-type sector collapse occurred in Holocene time. This sector collapse produced a voluminous volcanic debris avalanche which flowed south-southeast down the Chakachatna River valley (Plate 1-1). Following sector collapse, the Holocene

cones of Crater Peak and the present Mt. Spurr summit were built in the breached rim and in the collapsed summit depression, respectively (Figure 1-2).

Although we have rejected the caldera hypothesis, there is abundant evidence from our K-Ar dating of lava flows and from previous tephrachronologic work that an active magmatic system has been present during the late Pleistocene-to-Holocene time interval that is of critical interest for geothermal energy resource assessment. There are also several presently active geothermal manifestations in the area. These include previously-unreported zones of fumarolic activity on the flanks of the Mt. Spurr summit cone, photographic evidence of snow melt at the summit crater, a previously-undescribed 40°C warm spring south of Crater Peak, and the fumaroles and hot crater lake of Crater Peak.

A major portion of our project was devoted to exploration for accessible geothermal reservoirs on the south side of the Mt. Spurr area. Geophysical and geochemical surveys were conducted, in addition to the geologic mapping and geochronologic studies. Many coincident mercury and helium anomalies were found, indicating the presence of geothermal systems at depth.

The CSAMT data show a discontinuous, very low resistivity zone under several areas surveyed. The presence of low resistivity does not automatically indicate a geothermal reservoir. This zone could possibly be a cold, porous unit filled with saline or alkaline water or, alternatively, a clay-rich bed. However, the combination of other geothermal indicators (S-P, He and Hg soil anomalies) suggests strongly that the zone contains hot water. Figure 4-8 is a three-dimensional fence diagram with the very low resistivity zone shown in black. On the southeast flank of Crater Peak, this zone is roughly parallel to the present topography, only somewhat steeper.

This suggests it might have been part of a pre-Crater Peak cone. If so, it might be a porous tephra layer overlain by some sort of cap rock. Alternatively, based on the mapped outcrops of sedimentary rocks on the east side of the glacier (Plate 1-1), the low resistivity zone could be a sandstone unit.

The S-P survey on the side of Crater Peak shows some world-class anomalies. One, a dipole of +641 to -815 mV, is located in the vicinity of the uphill cut-off of the very low resistivity zone. In addition to the dipole anomaly, there are two negative and one positive anomalies in a linear, northeast-trending alignment that coincides with an abrupt cut-off in He soil gas anomalies (Plate 6-1). There is some indication of a reduction in large Hg anomalies in the same area, although this effect is not a sharp cut-off.

The combination of these various geothermal indicators strongly suggests that the low resistivity zone represents a geothermal reservoir with some sort of a linear cut-off occurring near the 3500 ft. contour line on the south slope of Crater Peak (Plate 6-1). The cut-off is on trend with a mapped fault to the east that juxtaposes Kenai group sediments and granitic basement (Plate 1-1). No evidence can be found for the fault in the deep north-south canyon that dissects the Crater Peak cone (Plate 6-1), indicating that, if present, the fault pre-dates the formation of the Holocene Crater Peak cone.

It is possible that the low resistivity zone could be a south-dipping Tertiary sandstone unit with an up-dip seal provided by sector collapse deposits, ancestral Spurr volcano lava flows, or flows from Crater Peak. The same argument can be made for a porous tephra layer deposited by the ancestral Mt. Spurr Volcano. In this model, sector collapse would remove the original up-dip part of the porous bed and it would later be covered with impermeable lava flows of the Crater Peak cone, thus providing an up-dip trap for geothermal water and/or steam.

Hill 2450 also has a pronounced S-P anomaly (+1000 to -1000 mV) underlain by a discontinuous, very low resistivity zone at a depth of about 1 km. There are only two He and Hg sample sites in this area, so we cannot as yet consider it as a probable geothermal reservoir; but it seems to be a promising area for future investigation.

Some of the other areas where He, Hg and CSAMT anomalies occur are also possible areas of geothermal interest. The very low resistivity anomaly suggested by the profiles C-C' (Figure 4-5) and D-D' (Figure 4-6) does not have the extensive S-P, Hg and He coverage of the southeast slope of Crater Peak. Thus it represents an area of possible interest, but cannot be considered a prime site without further investigation. The rather extreme topography at stations 1, 2 and 3 would tend to reduce the electric field (E), thus decreasing the apparent resistivity. However, the fact that the CSAMT data from site 3 show no low resistivity zone, at least to 4000 ft. depth, suggests that the topographic effect did not produce spurious low resistivity at the other stations. We cannot tell whether this zone connects with the anomaly at the south side of Crater Peak because there were no CSAMT stations (Figure 4-8 and Plate 6-1) between these widely separated areas.

Several important questions remain which our reconnaissance study cannot answer. If the low resistivity zone is a geothermal reservoir, either a tephra bed or a sandstone, what forms the cap rock for the reservoir? Could the inferred reservoir be self-capped by deposition of minerals? If the reservoir is very hot, could there be a steam phase beneath the low resistivity zone? Passive seismic surveying would be an excellent follow-on technique to explore for vapor-phase activity.

The CSAMT data of sections 9 and 10 (Figure 4-7) show around 10 Ω-m resistivity at a depth of 2500 ft., just above very high resistivity, which we

think is probably the granitic basement rock. There is one anomalous He value in that area. More work is needed in this area before a meaningful evaluation can be made.

There is no doubt that the Mt. Spurr summit is hot--fumarole fields and melted snow at 10,000 ft. are ample evidence. One can also easily see the thermal manifestations at the summit of Crater Peak--a hot lake, diffuse fumarole fields, and a single, very large fumarole. The newly documented 40°C hot spring and warm seeps in a mile-long zone below in the canyon south of Crater Peak show that some geothermal heat is also available on the lower flanks of the Spurr volcano. Based upon the location of low resistivity zones and the coincidence of S-P, He and Hg anomalies, we have determined target areas for further detailed study or drilling. Plate 6-1 shows these target areas, together with CSAMT profile section lines, S-P anomalies and He anomalies.

The results of this study indicate that a geothermal system on the south flank of Crater Peak should be accessible by drilling to about 2,000 ft. depth. Prior to any exploratory drilling, we strongly recommend a follow-on program of passive seismic surveying to evaluate the possible presence of a steam system, together with additional self-potential, helium and mercury surveys to better define the configuration and extent of probable reservoirs.

It is also evident that there is a strong volcanic hazard to be evaluated in considering any development on the south side of Mt. Spurr. This hazardous situation may require angle drilling of production wells from safer areas and placement of power generation facilities at a considerable distance from hazardous areas.

Two State of Alaska geothermal lease sales have been held in the Mt. Spurr area. The second sale was directly related to an earlier State

release of preliminary results from this study. Completion of our study now shows that the prospects for geothermal energy resources at Mt. Spurr are very positive. A companion report on the detailed geology and geochemistry of Spurr volcano is currently in preparation by Dr. C. J. Nye.

## ACKNOWLEDGEMENTS

Financial support for this study was provided by the U.S. Department of Energy, Grant No. DE-FG07-84ID12471. Field assistance was ably provided by William Witte, Carl Tobin, David Bratt and Ted Clarke.

APPENDIX A

# HELIUM SURVEYS

**PROJECT REPORT CPL-598-2**

**A SURVEY OF GEOTHERMAL PROSPECTS**
**PROJECT D.O.E. GEOTHERMAL**
**MOUNT SPURR, ALASKA**

**OCTOBER 2, 1985**

**Submitted to:**

**GEOPHYSICAL INSTITUTE**
**UNIVERSITY OF ALASKA**
**FAIRBANKS, ALASKA**

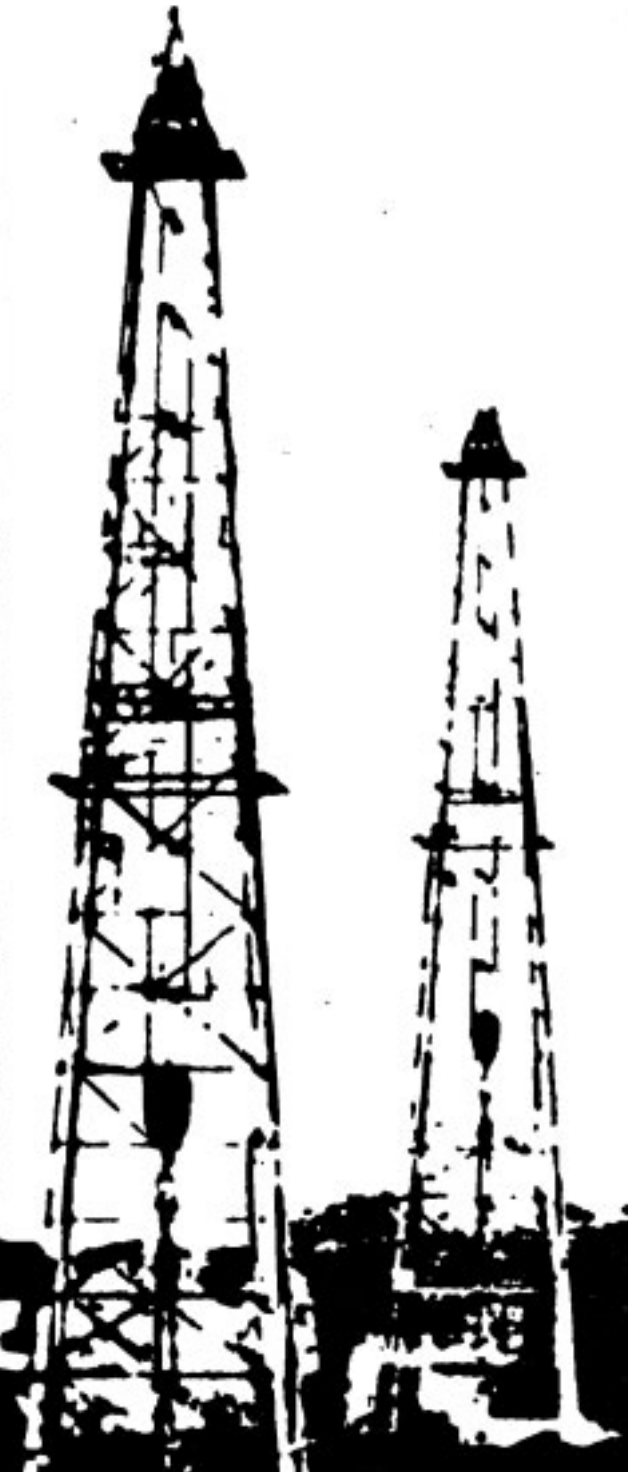

**URANIUM DEPOSITS**
**GEOTHERMAL ENERGY**
**PETROLEUM RESERVOIRS**

CP CHEMICAL PROJECTS LIMITED

TABLE OF CONTENTS



List of Tables



List of Figures



[1]Figure 1 has been replaced by Plate 5-2 in the Geophysical Institute report.

# 1. INTRODUCTION

During the period of July 30 to August 5, 1985, a helium survey was conducted over geothermal prospects in the Mount Spurr Area, Alaska.

This program was undertaken by the Geophysical Institute, University of Alaska, with the objective of finding whether there are any helium anomalies in the area under consideration.

An exploration crew from the Geophysical Institute collected 40 soil, 16 mud (water saturated soil) and 1 spring water sample during this program.

The analyses of the samples and the interpretation of the resulting data were performed at the geochemical laboratories of Chemical Projects Limited, Toronto, Ontario.

## 2. SURVEY TECHNIQUES

### 2.1 Sampling Methods

Forty soil, 16 mud (water saturated soil) and 1 spring water sample were collected in the Spurr Mountain area of Alaska. These samples were collected from random-spaced sampling stations, as indicated in Figure 1.

The soil, mud and water samples were preserved in hermetically sealed aluminum containers having a diameter of 1.5 inches and a length of 7 inches.

During the sampling procedure, the station barometric pressure, the air, soil and water temperatures and the sampling depth were measured and recorded at each sampling station.

### 2.2 Analytical Procedures

When the sealed containers with their contents were received at the laboratory, they were subjected to a period of equilibration at a constant temperature after which gas samples were extracted from each container and stored in Bistable gas samplers.

The gaseous contents of these Bistables were analyzed, employing a helium-hydrocarbon analyzer developed by Chemical Projects Limited, in order to determine the helium and hydrocarbon concentration in each sample. During the analysis, the concentration of helium in the sample was compared with that of standards which have helium concentrations of 5.20 ± 0.03 and 8.30 ± 0.05 ppm (by volume).

The practical detection limit for the helium analyses is 10 ppb (by volume) while that for the hydrocarbons, if present at concentrations of less than 10,000 ppm, is approximately 1 ppm (by volume). At higher concentrations exceeding 10,000 ppm, the detection limit is 500 ppm (by volume).

Since the helium concentration in the samples is a function of the soil and mud parameters, these were also determined for each sample. These data were used to correct the laboratory conditions back to those of the field at the time of sample collection.

## 3. RESULTS

### 3.1 Data Tables

The corrected helium, methane, ethane, ethene and propene (= propene + propane) results for the soil, mud and water samples are listed in Tables 1, 2 and 3. Also included in these tables are the statistical parameters and ordered listings of the helium values for the soil and mud samples.

In these tables and in the histogram, the following nomenclature is used:

Table 1 (Soil Samples)

| | | |
|---|---|---|
| Sample Number | = | The number that was assigned to each soil sample by the Geophysical Institute. |
| Depth | = | The reported soil depth (in inches) from which the sample was collected. |
| Helium | = | The concentration of helium in the gas of the soil micropores, expressed in ppm He (by volume). |
| Methane<br>Ethane<br>Ethene<br>Propane<br>Propene | = | The concentration of each of these hydrocarbon gases in the soil sample. Each concentration is expressed as $cm^3$ gas at NTP/gm of soil and has been multiplied by a factor of $10^8$. |

Table 2 (Mud Samples)

| | | |
|---|---|---|
| Sample Number | = | The number that was assigned to each mud sample by the Geophysical Institute. |

COMPANY :GEOPHYSICAL INSTITUTE
PROJECT :Alaska, D.O.E. Geothermal
DATE :AUGUST 28,1985

CHEMICAL PROJECTS LTD.

TABLE 1



SOIL SAMPLES :(S85TR-1H TO S85Jr-44H)

(*)-CONCENTRATIONS OF HYDROCARBONS ARE IN (CC GAS AT NTP/GRAM OF SOIL) x E-08

| SAMPLE NUMBER | DEPTH (IN) | HELIUM (ppmv) | METHANE (*) | ETHANE (*) | ETHENE (*) | PROPANE &PROPENE(*) | COUNTER |
|---|---|---|---|---|---|---|---|
| S85TR-1H | 18 | 5.97 | 99 | 0 | 230 | 66 | 1 |
| S85TR-2H | 10 | 5.10 | 324 | 0 | 130 | 97 | 2 |
| S85TR-4H | 18 | 7.98 | 94 | 0 | 24 | 0 | 3 |
| S85TR-5H | 14 | 6.78 | 76 | 0 | 0 | 0 | 4 |
| S85TR-7H | 14 | 9.60 | 657 | 0 | 0 | 53 | 5 |
| S85TR-10H | 14 | 5.64 | 84 | 0 | 0 | 0 | 6 |
| S85TR-11H | 18 | 5.37 | 111 | 0 | 0 | 0 | 7 |
| S85TR-12H | 24 | 5.26 | 111 | 0 | 0 | 0 | 8 |
| S85TR-13H | 18 | 6.61 | 274 | 0 | 1040 | 110 | 9 |
| S85Jr-3H | 20 | 10.3 | 74 | 0 | 37 | 0 | 10 |
| S85Jr-5H | 12 | 6.70 | 137 | 0 | 50 | 25 | 11 |
| S85Jr-6H | 24 | 6.55 | 315 | 0 | 90 | 90 | 12 |
| S85Jr-7H | 30 | 9.13 | 85 | 0 | 0 | 0 | 13 |
| S85Jr-9H | 24 | 5.89 | 229 | 0 | 274 | 0 | 14 |
| S85Jr-10H | 24 | 1.37 | 418 | 0 | 1590 | 251 | 15 |

CHEMICAL PROJECTS LTD.

TABLE 1



SOIL SAMPLES :(S85TR-1H TO S85Jr-44H)

(*)-CONCENTRATIONS OF HYDROCARBONS ARE IN (CC GAS AT NTP/GRAM OF SOIL) x E-08

| SAMPLE NUMBER | DEPTH (IN) | HELIUM (ppmv) | METHANE (*) | ETHANE (*) | ETHENE (*) | PROPANE &PROPENE (*) | COUNTER |
|---|---|---|---|---|---|---|---|
| S85Jr-12H | 30 | 6.41 | 94 | 0 | 94 | 0 | 16 |
| S85Jr-13H | 24 | 5.25 | 72 | 0 | 0 | 0 | 17 |
| S85Jr-14H | 15 | 6.31 | 123 | 0 | 31 | 0 | 18 |
| S85Jr-15H | 18 | 5.54 | 88 | 0 | 132 | 0 | 19 |
| S85Jr-16H | 15 | 5.41 | 69 | 0 | 0 | 0 | 20 |
| S85Jr-17H | 24 | 5.32 | 70 | 0 | 35 | 0 | 21 |
| S85Jr-19H | 24 | 5.42 | 122 | 0 | 0 | 0 | 22 |
| S85Jr-20H | 24 | 6.76 | 139 | 0 | 47 | 0 | 23 |
| S85Jr-21H | 20 | 6.96 | 1540 | 110 | 1540 | 220 | 24 |
| S85Jr-22H | 24 | 8.39 | 99 | 0 | 50 | 0 | 25 |
| S85Jr-25H | 20 | 6.37 | 204 | 0 | 82 | 0 | 26 |
| S85Jr-26H | 24 | 5.50 | 176 | 0 | 235 | 0 | 27 |
| S85Jr-28H | 15 | 5.51 | 75 | 0 | 0 | 0 | 28 |
| S85Jr-29H | 18 | 5.86 | 1010 | 0 | 112 | 0 | 29 |
| S85Jr-30H | 14 | 5.48 | 81 | 0 | 0 | 0 | 30 |

COMPANY :GEOPHYSICAL INSTITUTE
PROJECT :Alaska, D.O.E. Geothermal
DATE :AUGUST 28,1985

CHEMICAL PROJECTS LTD.

TABLE 1



SOIL SAMPLES :(S85TR-1H TO S85Jr-44H)

(*)-CONCENTRATIONS OF HYDROCARBONS ARE IN (CC GAS AT NTP/GRAM OF SOIL) x E-08

| SAMPLE NUMBER | DEPTH (IN) | HELIUM (ppmv) | METHANE (*) | ETHANE (*) | ETHENE (*) | PROPANE &PROPENE(*) | COUNTER |
|---|---|---|---|---|---|---|---|
| S85Jr-31H | 12 | 10.8 | 65 | 0 | 0 | 0 | 31 |
| S85Jr-32H | 18 | 10.1 | 61 | 0 | 61 | 0 | 32 |
| S85Jr-33H | 18 | 3.51 | 4440 | 617 | 556 | 556 | 33 |
| S85Jr-34H | 34 | 5.67 | 85 | 0 | 0 | 0 | 34 |
| S85Jr-35H | 24 | 5.34 | 82 | 0 | 0 | 0 | 35 |
| S85Jr-36H | 24 | 5.63 | 86 | 0 | 214 | 0 | 36 |
| S85Jr-38H | 15 | 7.92 | 460 | 0 | 138 | 0 | 37 |
| S85Jr-39H | 15 | 5.83 | 66 | 0 | 33 | 0 | 38 |
| S85Jr-40H | 15 | 9.29 | 182 | 0 | 73 | 0 | 39 |
| S85Jr-44H | 18 | 12.8 | 151 | 0 | 377 | 75 | 40 |

TABLE 1

HELIUM VALUES IN ASCENDING ORDER

| | | | | | | | | | | | |
|---|---|---|---|---|---|---|---|---|---|---|---|
| S85Jr-10H | 1.37 | | S85Jr-30H | 5.48 | | S85TR-1H | 5.97 | | S85Jr-38H | 7.92 | |
| S85Jr-33H | 3.51 | | S85Jr-26H | 5.50 | | S85Jr-14H | 6.31 | | S85TR-4H | 7.98 | |
| S85TR-2H | 5.10 | | S85Jr-28H | 5.51 | | S85Jr-25H | 6.37 | | S85Jr-22H | 8.39 | |
| S85Jr-13H | 5.25 | | S85Jr-15H | 5.54 | | S85Jr-12H | 6.41 | | S85Jr-7H | 9.13 | |
| S85TR-12H | 5.26 | | S85Jr-36H | 5.63 | | S85Jr-6H | 6.55 | | S85Jr-40H | 9.29 | |
| S85Jr-17H | 5.32 | | S85TR-10H | 5.64 | | S85TR-13H | 6.61 | | S85TR-7H | 9.60 | |
| S85Jr-35H | 5.34 | | S85Jr-34H | 5.67 | | S85Jr-5H | 6.70 | | S85Jr-32H | 10.1 | |
| S85TR-11H | 5.37 | | S85Jr-39H | 5.83 | | S85Jr-20H | 6.76 | | S85Jr-3H | 10.3 | |
| S85Jr-16H | 5.41 | | S85Jr-29H | 5.86 | | S85TR-5H | 6.78 | | S85Jr-31H | 10.8 | |
| S85Jr-19H | 5.42 | | S85Jr-9H | 5.89 | | S85Jr-21H | 6.96 | | S85Jr-44H | 12.8 | |

COMPANY :GEOPHYSICAL INSTITUTE
PROJECT :Alaska, D.O.E. Geothermal
DATE :AUGUST 28,1985

TABLE 1

SOIL SAMPLE : (S85TR-1H TO S85Jr-44H)

STATISTICAL PARAMETERS

HELIUM VALUES

| | NUMBER | MEAN | MEDIAN | STANDARD DEVIATION | VARIANCE |
|---|---|---|---|---|---|
| TOTAL POPULATION | 40 | 6.64 | 5.93 | 2.10 | 4.40 |
| BACKGROUND POPULATION | 26 | 5.47 | 5.53 | 1.03 | 1.06 |

ANOMALY RANGE

| | | | |
|---|---|---|---|
| > 4 S.D. | > | 9.59 | |
| > 3-4 S.D. | 8.57 | - | 9.59 |
| > 2-3 S.D. | 7.54 | - | 8.56 |
| > 1-2 S.D. | 6.51 | - | 7.53 |

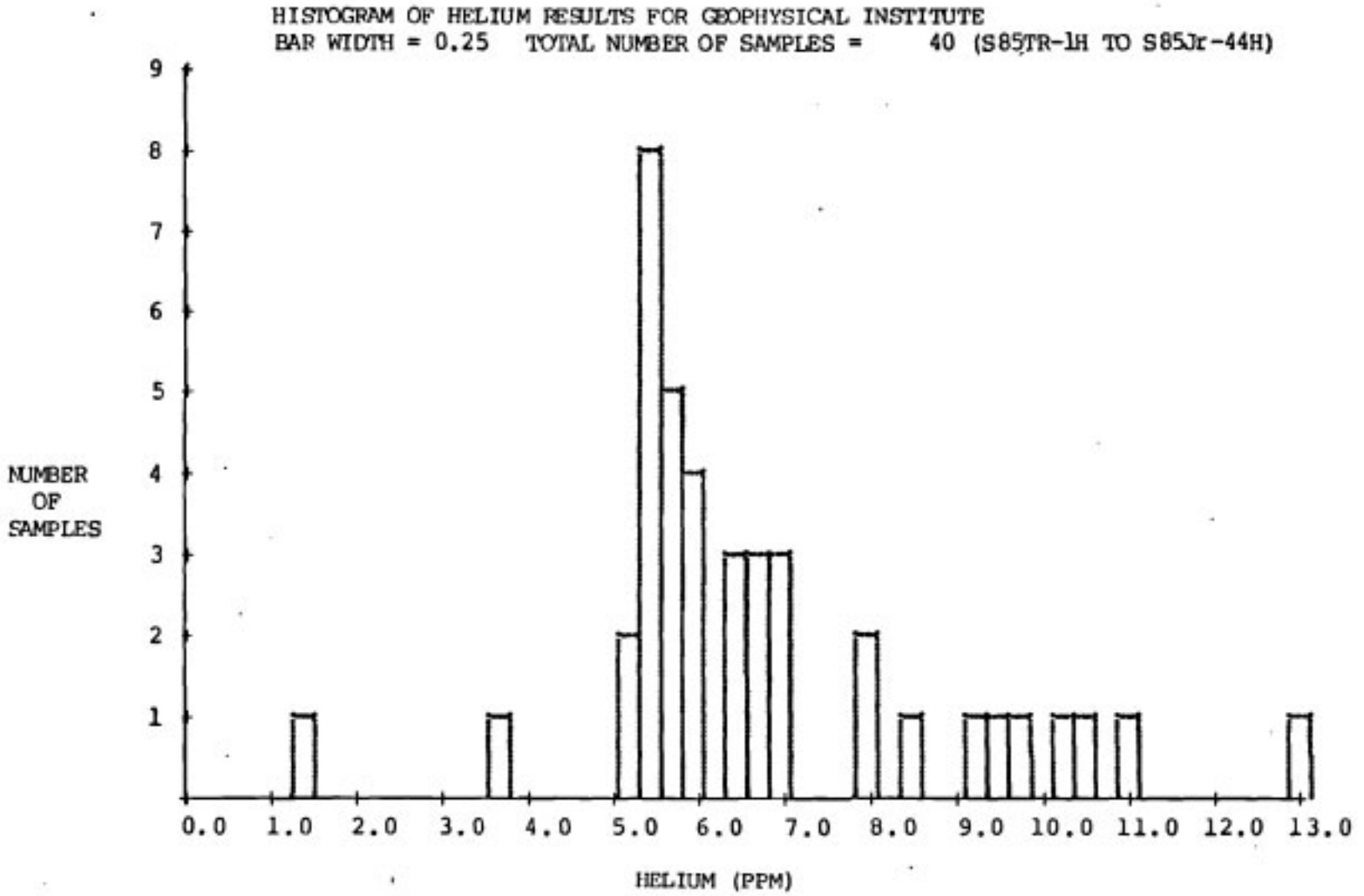
HISTOGRAM OF HELIUM RESULTS FOR GEOPHYSICAL INSTITUTE
BAR WIDTH = 0.25 TOTAL NUMBER OF SAMPLES = 40 (S85TR-1H TO S85Jr-44H)
NUMBER OF SAMPLES
9
8
7
6
5
4
3
2
1
0.0 1.0 2.0 3.0 4.0 5.0 6.0 7.0 8.0 9.0 10.0 11.0 12.0 13.0
HELIUM (PPM)

TABLE 1

METHANE VALUES IN ASCENDING ORDER

| | | | | | | | |
|---|---|---|---|---|---|---|---|
| S85Jr-32H | 61 | S85Jr-35H | 82 | S85TR-12H | 111 | S85Jr-9H | 229 |
| S85Jr-31H | 65 | S85TR-10H | 84 | S85TR-11H | 111 | S85TR-13H | 274 |
| S85Jr-39H | 66 | S85Jr-34H | 85 | S85Jr-19H | 122 | S85Jr-6H | 315 |
| S85Jr-16H | 69 | S85Jr-7H | 85 | S85Jr-14H | 123 | S85TR-2H | 324 |
| S85Jr-17H | 70 | S85Jr-36H | 86 | S85Jr-5H | 137 | S85Jr-10H | 418 |
| S85Jr-13H | 72 | S85Jr-15H | 88 | S85Jr-20H | 139 | S85Jr-38H | 460 |
| S85Jr-3H | 74 | S85Jr-12H | 94 | S85Jr-44H | 151 | S85TR-7H | 657 |
| S85Jr-28H | 75 | S85TR-4H | 94 | S85Jr-26H | 176 | S85Jr-29H | 1010 |
| S85TR-5H | 76 | S85Jr-22H | 99 | S85Jr-40H | 182 | S85Jr-21H | 1540 |
| S85Jr-30H | 81 | S85TR-1H | 99 | S85Jr-25H | 204 | S85Jr-33H | 4440 |

COMPANY :GEOPHYSICAL INSTITUTE
PROJECT :Alaska, D.O.E. Geothermal
DATE :AUGUST 28,1985

TABLE 1

SOIL SAMPLE : (S85TR-1H TO S85Jr-44H)

## STATISTICAL PARAMETERS

### METHANE VALUES

| | NUMBER | MEAN | MEDIAN | STANDARD DEVIATION | VARIANCE |
|---|---|---|---|---|---|
| TOTAL POPULATION | 40 | 318.20 | 105.00 | 726.03 | 527113.65 |
| BACKGROUND POPULATION | 33 | 117.55 | 94.00 | 62.07 | 3852.32 |

## ANOMALY RANGE

| | | | |
|---|---|---|---|
| > 4 S.D. | > | 365.83 | |
| > 3-4 S.D. | 303.77 | - | 365.83 |
| > 2-3 S.D. | 241.70 | - | 303.76 |
| > 1-2 S.D. | 179.63 | - | 241.69 |

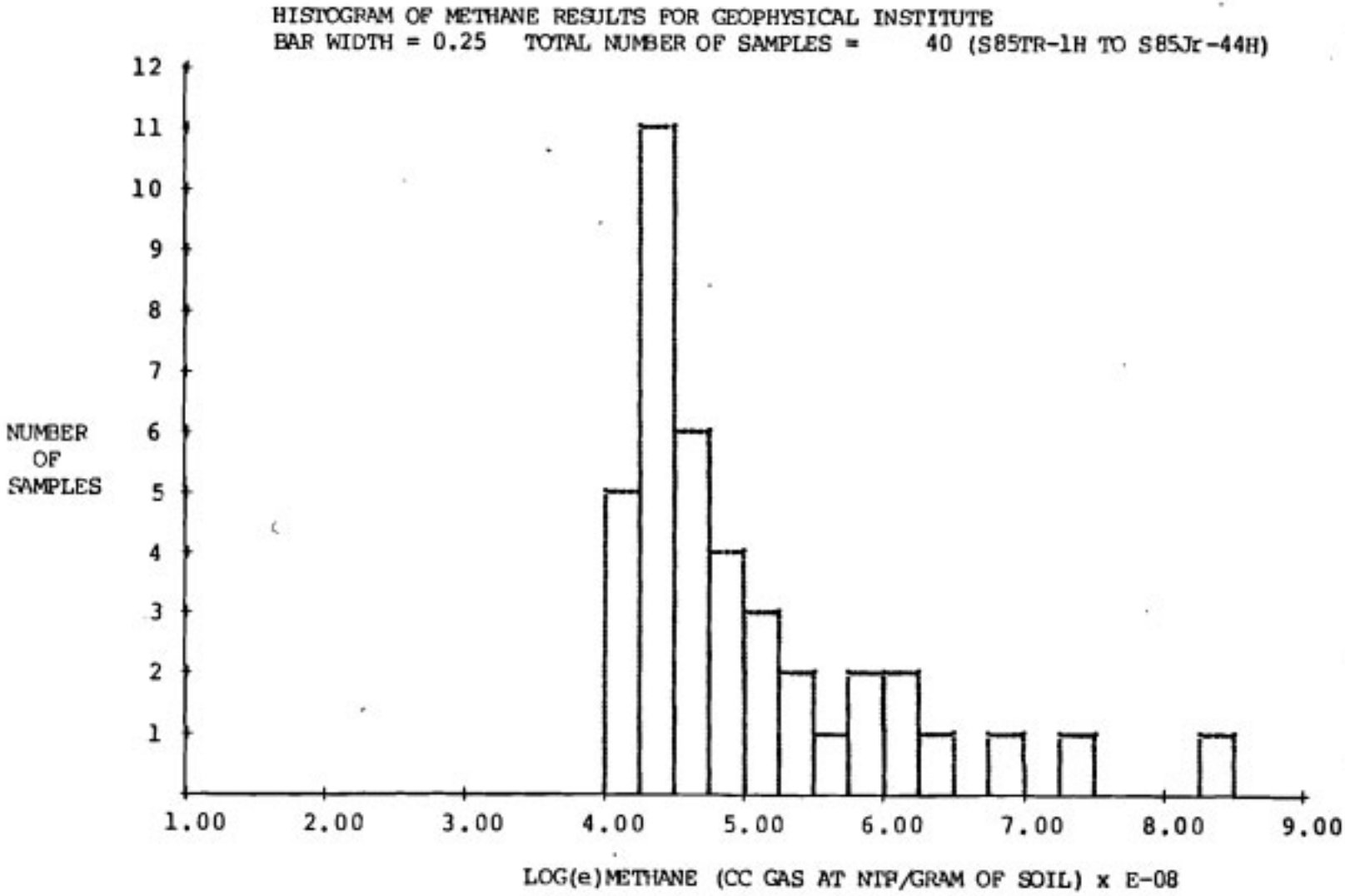
HISTOGRAM OF METHANE RESULTS FOR GEOPHYSICAL INSTITUTE
BAR WIDTH = 0.25 TOTAL NUMBER OF SAMPLES = 40 (S85TR-1H TO S85Jr-44H)
NUMBER OF SAMPLES
12
11
10
9
8
7
6
5
4
3
2
1
1.00
2.00
3.00
4.00
5.00
6.00
7.00
8.00
9.00
LOG(e)METHANE (CC GAS AT NTP/GRAM OF SOIL) x E-08

COMPANY :GEOPHYSICAL INSTITUTE
PROJECT :Alaska, D.O.E. Geothermal
DATE :AUGUST 28,1985

CHEMICAL PROJECTS LTD.

TABLE 2



MUD SAMPLES :(S85TR-3H TO S85Jr-46H)

(*)-CONCENTRATIONS OF ALL GASES ARE IN (CC GAS AT NTP/CC OF MUD) x E-08

| SAMPLE NUMBER | DEPTH (IN) | HELIUM (*) | METHANE (*) | ETHANE (*) | ETHENE (*) | PROPENE (*) | COUNTER |
|---|---|---|---|---|---|---|---|
| S85TR-3H | 12 | 9.36 | 30 | 0 | 30 | 0 | 1 |
| S85TR-6H | 18 | 26.8 | 931 | 0 | 54 | 0 | 2 |
| S85Jr-1H | 12 | 11.2 | 266 | 0 | 243 | 0 | 3 |
| S85Jr-2H | 17 | 7.19 | 344 | 0 | 453 | 177 | 4 |
| S85Jr-4H | 15 | 10.4 | 2 | 0 | 0 | 0 | 5 |
| S85Jr-11H | 30 | 18.5 | 4 | 0 | 215 | 0 | 6 |
| S85Jr-18H | 12 | 8.40 | 123 | 0 | 22 | 0 | 7 |
| S85Jr-23H | 24 | 6.95 | 2 | 0 | 17 | 0 | 8 |
| S85Jr-24H | 24 | 11.0 | 2 | 0 | 0 | 0 | 9 |
| S85Jr-27H | 18 | 22.4 | 4 | 0 | 68 | 0 | 10 |
| S85Jr-37H | 24 | 15.0 | 195 | 0 | 716 | 54 | 11 |
| S85Jr-41H | 24 | 8.04 | 3 | 0 | 163 | 0 | 12 |
| S85Jr-42H | 15 | 23.4 | 274 | 0 | 2250 | 98 | 13 |
| S85Jr-43H | 18 | 39.5 | 8 | 0 | 1320 | 114 | 14 |
| S85Jr-45H | 18 | 6.66 | 701 | 0 | 560 | 80 | 15 |

COMPANY :GEOPHYSICAL INSTITUTE
PROJECT :Alaska, D.O.E. Geothermal
DATE :AUGUST 28,1985

CHEMICAL PROJECTS LTD.

TABLE 2



MUD SAMPLES :(S85TR-3H TO S85Jr-46H)

(*)-CONCENTRATIONS OF ALL GASES ARE IN (CC GAS AT NTP/CC OF MUD) x E-08

| SAMPLE NUMBER | DEPTH (IN) | HELIUM (*) | METHANE (*) | ETHANE (*) | ETHENE (*) | PROPENE (*) | COUNTER |
|---|---|---|---|---|---|---|---|
| S85Jr-46H | 24 | 16.7 | 3 | 0 | 386 | 0 | 16 |

COMPANY :GEOPHYSICAL INSTITUTE
PROJECT :Alaska, D.O.E. Geothermal
DATE :AUGUST 28,1985


TABLE 2

HELIUM VALUES IN ASCENDING ORDER

| | | | | | | | | | | | |
|---|---|---|---|---|---|---|---|---|---|---|---|
| S85Jr-45H | 6.66 | | S85Jr-18H | 8.40 | | S85Jr-1H | 11.2 | | S85Jr-27H | 22.4 | |
| S85Jr-23H | 6.95 | | S85TR-3H | 9.36 | | S85Jr-37H | 15.0 | | S85Jr-42H | 23.4 | |
| S85Jr-2H | 7.19 | | S85Jr-4H | 10.4 | | S85Jr-46H | 16.7 | | S85TR-6H | 26.8 | |
| S85Jr-41H | 8.04 | | S85Jr-24H | 11.0 | | S85Jr-11H | 18.5 | | S85Jr-43H | 39.5 | |

COMPANY :GEOPHYSICAL INSTITUTE
PROJECT :Alaska, D.O.E. Geothermal
DATE :AUGUST 28,1985

TABLE 2

MUD SAMPLE : (S85TR-3H TO S85Jr-46H)

## STATISTICAL PARAMETERS

### HELIUM VALUES

| | NUMBER | MEAN | MEDIAN | STANDARD DEVIATION | VARIANCE |
|---|---|---|---|---|---|
| TOTAL POPULATION | 16 | 15.09 | 11.10 | 9.13 | 83.37 |
| BACKGROUND POPULATION | 10 | 9.42 | 8.88 | 2.57 | 6.60 |

## ANOMALY RANGE

| | | | |
|---|---|---|---|
| > 4 S.D. | > | 19.70 | |
| > 3-4 S.D. | 17.14 | - | 19.70 |
| > 2-3 S.D. | 14.57 | - | 17.13 |
| > 1-2 S.D. | 12.00 | - | 14.56 |

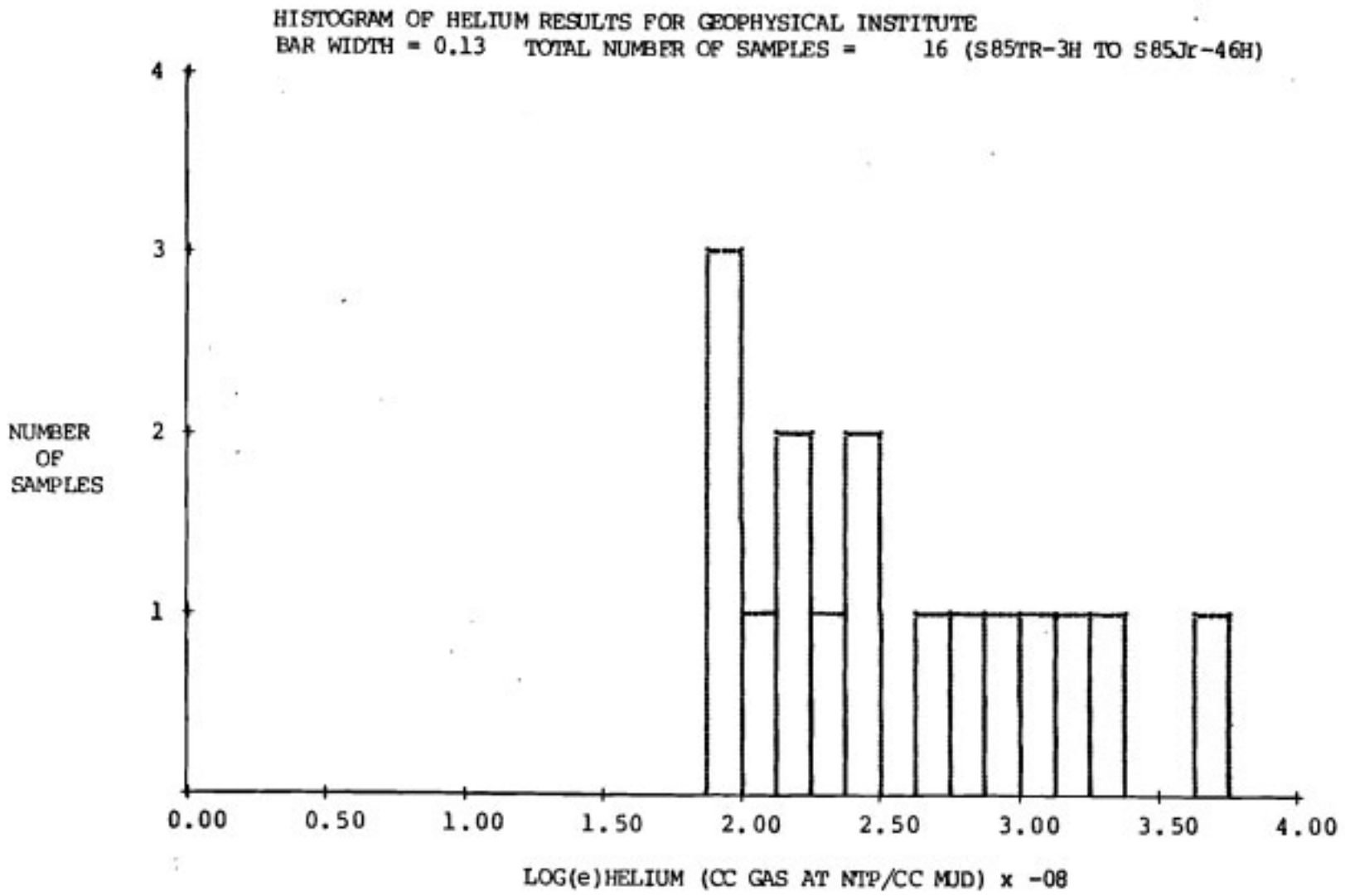
HISTOGRAM OF HELIUM RESULTS FOR GEOPHYSICAL INSTITUTE
BAR WIDTH = 0.13 TOTAL NUMBER OF SAMPLES = 16 (S85TR-3H TO S85Jr-46H)
NUMBER OF SAMPLES
4
3
2
1
0.00
0.50
1.00
1.50
2.00
2.50
3.00
3.50
4.00
LOG(e)HELIUM (CC GAS AT NTP/CC MUD) x -08

COMPANY :GEOPHYSICAL INSTITUTE
PROJECT :Alaska, D.O.E. Geothermal
DATE :AUGUST 28,1985
PAGE : 1

TABLE 2

METHANE VALUES IN ASCENDING ORDER

| | | | | | | | |
|---|---|---|---|---|---|---|---|
| S85Jr-24H | 2 | S85Jr-46H | 3 | S85TR-3H | 30 | S85Jr-42H | 274 |
| S85Jr-23H | 2 | S85Jr-27H | 4 | S85Jr-18H | 123 | S85Jr-2H | 344 |
| S85Jr-4H | 2 | S85Jr-11H | 4 | S85Jr-37H | 195 | S85Jr-45H | 701 |
| S85Jr-41H | 3 | S85Jr-43H | 8 | S85Jr-1H | 266 | S85TR-6H | 931 |

COMPANY :GEOPHYSICAL INSTITUTE
PROJECT :Alaska, D.O.E. Geothermal
DATE :AUGUST 28,1985

TABLE 2

MUD SAMPLE : (S85TR-3H TO S85Jr-46H)

STATISTICAL PARAMETERS

METHANE VALUES

| | NUMBER | MEAN | MEDIAN | STANDARD DEVIATION | VARIANCE |
|---|---|---|---|---|---|
| TOTAL POPULATION | 16 | 180.75 | 19.00 | 277.34 | 76918.73 |
| BACKGROUND POPULATION | 10 | 18.10 | 3.50 | 37.83 | 1430.99 |

ANOMALY RANGE

| | | | |
|---|---|---|---|
| > 4 S.D. | > | 169.42 | |
| > 3-4 S.D. | 131.60 | - | 169.42 |
| > 2-3 S.D. | 93.77 | - | 131.59 |
| > 1-2 S.D. | 55.94 | - | 93.76 |

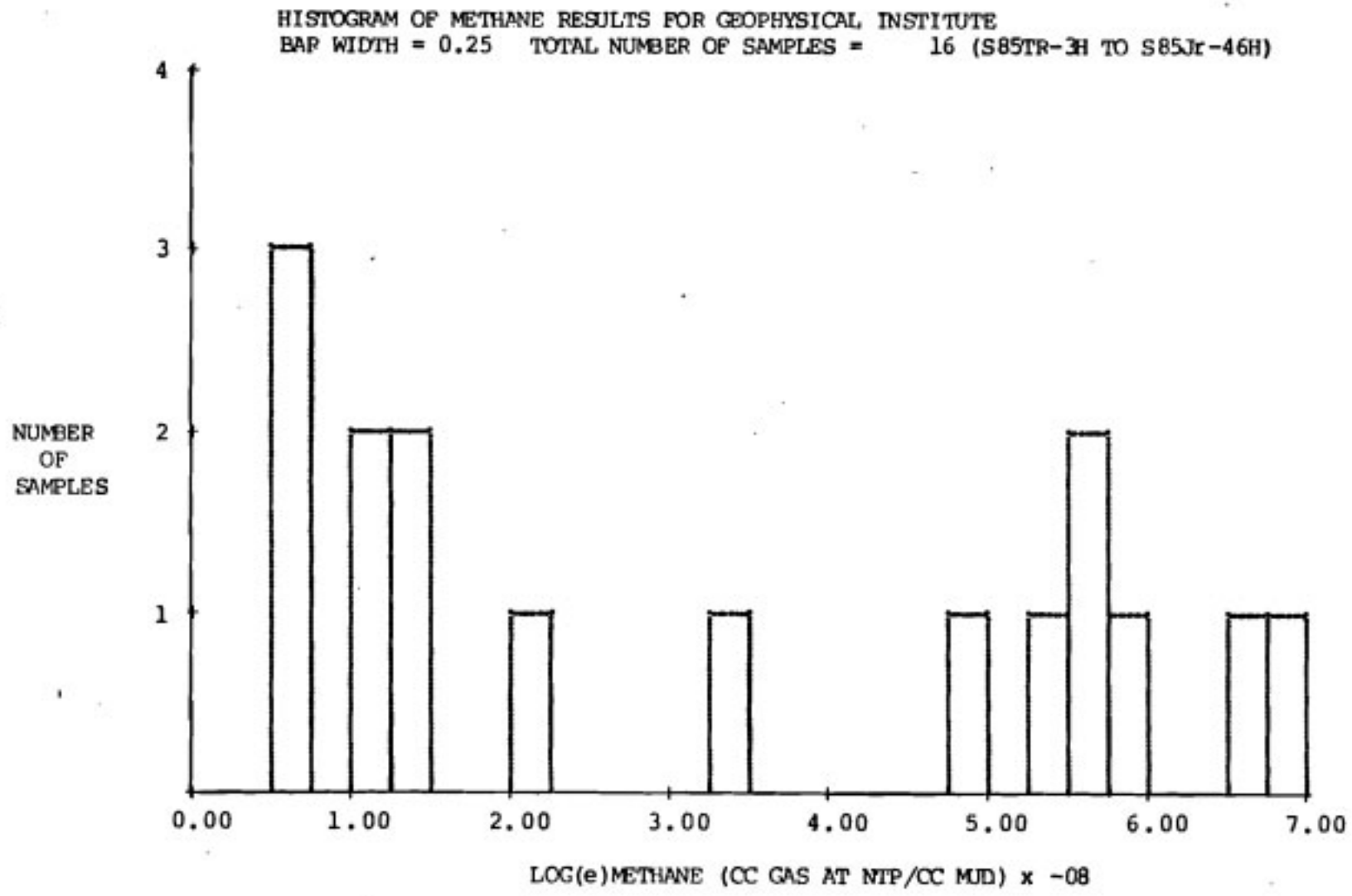
HISTOGRAM OF METHANE RESULTS FOR GEOPHYSICAL INSTITUTE
BAR WIDTH = 0.25 TOTAL NUMBER OF SAMPLES = 16 (S85TR-3H TO S85Jr-46H)
NUMBER OF SAMPLES
4
3
2
1
0.00
1.00
2.00
3.00
4.00
5.00
6.00
7.00
LOG(e)METHANE (CC GAS AT NTP/CC MUD) x -08

COMPANY :GEOPHYSICAL INSTITUTE
PROJECT :Alaska, D.O.E. Geothermal
DATE :AUGUST 28,1985

CHEMICAL PROJECTS LTD.
TABLE 3



WATER SAMPLES :S85Jr-8H
(*)-CONCENTRATION OF GASES IN (CC GAS AT NTP/CC WATER) x E-08

| SAMPLE NUMBER | DEPTH (ft) | WATER TEMP. (°C) | HELIUM (*) | METHANE (*) | ETHANE (*) | ETHENE (*) | PROPENE (*) | COUNTER |
|---|---|---|---|---|---|---|---|---|
| S85Jr-8H | Surface | 37 | 4.12 | 34 | 0 | 0 | 0 | 1 |

Depth = The reported depth (in inches) from which the sample was collected.

Helium = The concentration of helium in the mud or sediment samples which was dissolved in the interstitial soil water and bubble phase of the sample. Each concentration is expressed as $cm^3$ He at NTP/$cm^3$ mud and has been multiplied by a factor of $10^8$.

Helium Log (e) = The natural ($log_e$) of the concentration of helium present in the mud samples.

Methane
Ethane
Ethene
Propane
Propene
= The concentration of each of these gases present in the mud sample. Each concentration is expressed as $cm^3$ gas at NTP/$cm^3$ mud and has been multiplied by a factor of $10^8$.

Table 3 (Water Sample)

Sample Number = The number that was assigned to each water sample by the Geophysical Institute.

Depth = The reported depth (in feet) at which the sample was collected.

Helium = The concentration of helium dissolved in the sample water expressed as $cm^3$ He at NTP/$cm^3$ $H_2O$. In this table each dissolved helium value has been multiplied by a factor of $10^8$.

Water Temperature = The temperature of the sample water expressed in °C.

| | | |
|---|---|---|
| Methane | = | The concentration of each of these gases dissolved in the sample water. Each concentration is expressed as $cm^3$ gas at NTP/ $cm^3$ $H_2O$ and it has also been multiplied by a factor of $10^8$. |
| Ethane | | |
| Ethene | | |
| Propene | | |

## 3.2 Statistical Evaluation of the Data

The soil samples and the mud samples were examined statistically. The two sets of data were treated in the same manner. The determination of the background for the data set was commenced by first sorting and listing the results ($X_i$) in ascending order. The mean ($\overline{X}_T$) was then calculated for the entire set of values. The subset of data having values equal to or less than $\overline{X}_T$ was then defined. The mean ($\overline{X}_b$) and standard deviation ($S_b$) for this subset were calculated and estimated to be the background mean and standard deviation. Anomalous values were assumed to be those results that exceeded the background mean by more than one standard deviation of the background population, that is, data greater than $\overline{X}_b + S_b$ were taken as being anomalous. In terms of $Z_i = (X_i - \overline{X}_b)/S_b$, anomalous values correspond to those of which $Z_i > 1$.

The anomalous values in each data set were ordered as indicated below into four categories according to the number of background standard deviation ($S_b$) by which they exceeded the background mean. Increasingly anomalous categories are shown by colour coding in the following manner:

| Range of Values (In values of $Z_i$ or the number of standard deviation ($S_b$) that the data exceed the background mean ($\overline{X}_b$)) | Colour Code |
|---|---|
| > 4 S.D. | Red |
| > 3 - 4 S.D. | Orange |
| > 2 - 3 S.D. | Yellow |
| > 1 - 2 S.D. | Green |

## 3.3 Maps

The sampling locations and helium results for the 40 soil, 16 mud and 1 water sample collected in this survey are plotted in Figure 1 (map pocket). This map was prepared from a sample location map and a topo map supplied by the Geophysical Institute. One mylar copy of Figure 1 and two mylar copies of the pertinent topo map are included in the map roll.

On this map, the soil sampling locations are designated as hollow circles, the mud sampling locations are designated as squares and the spring water sample location is designated as a triangle. The soil and mud samples are coloured to accentuate anomalous helium values, as described in Section 3.2.

Each helium concentration is marked in a larger type at the site of the appropriate sampling location while the number assigned to each sampling station is given in a smaller type.

## 4. COMMENTS AND RECOMMENDATIONS

This helium survey consists of 57 samples. The sample population can be divided into three groups:

Group 1 - 40 soil samples (samples in which the micropores contain a gas phase)

Group 2 - 16 mud samples (soil samples in which the micropores are completely filled with water)

Group 3 - 1 water sample (a sample of water collected from a free-flowing hot spring)

The first two groups of samples have been treated statistically as separate groups. Each of these two groups has its characteristic range of helium and hydrocarbon values. The individual helium and hydrocarbon values are comparable within each specific group but not outside of a given group. In order to compare helium levels in soil and mud, the data obtained are presented in Figure 1 in terms of standard deviations above the background mean.

The results indicate that the mean value of helium in the background population is 5.47 units for the soil samples and 9.42 units for the mud samples. These values are slightly higher than normal helium background levels. The background values indicate that the sampling grid was not large enough to fully extend beyond the anomalous areas. The range of helium values in the soil samples vary from 1.37 to 12.8 units and in the mud samples from 6.66 to 39.5 units. The mean background value of methane is 117.55 units for the soil samples and 9.42 units for the mud samples. The range of methane values in the soil samples vary from 60 to 4440 units and in the mud samples from 2 to 931 units. The methane values quoted are within the range of methane levels which can be generated close to the surface by biogenic activity.

A number of samples contain low concentrations of hydrocarbons of the $C_2$ and $C_3$ series. The low values of helium (1.37 units at station Jr-10 and 3.51 units at station Jr-33) are probably due to the depressing effect of hydrocarbon emanations in the ground. It is likely that these emanations exceed the rate of the helium flux at the above stations. Helium highs extending from station Jr-31 to station TR-7 and station Jr-27 to station Jr-42 may indicate probable fault lines and hot spots. The helium anomaly at Jr-11 suggests the presence of a hot spot in this area. The water sample collected at station Jr-8 has a low helium value (4.12 units) and a hydrocarbon value (methane 34 units). This low helium value may have resulted either from helium and hydrocarbons escaping prior to sample collection or because the water flow rate was greater than the helium emanation rate.

There are a number of points that would be of help in data interpretation. These include:

1. determination of helium flux in near-subsurface as a function of depth. This could be accomplished by collecting soil samples at 3 different depths, e.g. 12", 24" and 36".

2. determination of helium and hydrocarbon, etc. levels in gas emanation near hot springs, geysers and in volcano craters.

We suggest these points for possible inclusion in future work.